Natural killer cell-mediated cytotoxicity shapes the clonal evolution of B-cell leukemia

Buri, M.C.; Shoeb, M.R.; Bykov, A.; Repiscak, P.; Baik, H.; Dupanovic, A.; ... ; Putz, E.M.

Natural Killer Cell–Mediated Cytotoxicity Shapes the Clonal Evolution of B-cell Leukemia

Michelle C. Buri[1], Mohamed R. Shoeb[1], Aleksandr Bykov[1], Peter Repiscak[1], Hayeon Baik[1], Alma Dupanovic[1], Faith O. David[1,2], Boris Kovacic[1], Faith Hall-Glenn[1], Sara Dopa[1,3], Jos Urbanus[4], Lisa Sippl[1], Susanne Stofner[1], Dominik Emminger[1,5], Jason Cosgrove[6], Dagmar Schinnerl[1], Anna R. Poetsch[7], Manfred Lehner[1,5], Xaver Koenig[3], Leïla Perié[6], Ton N. Schumacher[4,8], Dagmar Gotthardt[9], Florian Halbritter[1], and Eva M. Putz[1,2]

ABSTRACT

The term cancer immunoediting describes the dual role by which the immune system can suppress and promote tumor growth and is divided into three phases: elimination, equilibrium, and escape. The role of NK cells has mainly been attributed to the elimination phase. Here, we show that NK cells play a role in all three phases of cancer immunoediting. Extended co-culturing of DNA-barcoded mouse BCR/ABL^{p185+} B-cell acute lymphoblastic leukemia (B-ALL) cells with NK cells allowed for a quantitative measure of NK cell–mediated immunoediting. Although most tumor cell clones were efficiently eliminated by NK cells, a certain fraction of tumor cells harbored an intrinsic primary resistance. Furthermore, DNA barcoding revealed tumor cell clones with secondary resistance, which stochastically acquired resistance to NK cells. NK cell–mediated cytotoxicity put a selective pressure on B-ALL cells, which led to an outgrowth of primary and secondary resistant tumor cell clones, which were characterized by an IFNγ signature. Besides well-known regulators of immune evasion, our analysis of NK cell–resistant tumor cells revealed the upregulation of genes, including lymphocyte antigen 6 complex, locus A (*Ly6a*), which we found to promote leukemic cell resistance to NK cells. Translation of our findings to the human system showed that high expression of *LY6E* on tumor cells impaired their physical interaction with NK cells and led to worse prognosis in patients with leukemia. Our results demonstrate that tumor cells are actively edited by NK cells during the equilibrium phase and use different avenues to escape NK cell–mediated eradication.

Introduction

Cancer immunoediting refers to the dynamic interaction between immune and cancer cells during tumor development (1). The immune system can have both tumor-promoting and tumor-suppressive effects. This process occurs in three phases: elimination, equilibrium, and escape. In the elimination phase, adaptive and innate immune cells, particularly cytotoxic T cells and NK cells, recognize and eliminate cancer cells. The equilibrium phase involves the coexistence of tumor cells and the immune system, leading to sculpting of the tumor under constant immune pressure, ultimately resulting in immune escape (2).

NK cells are innate lymphoid cells with the ability to recognize and eliminate damaged, stressed, and infected cells, including cancer cells (3). NK-cell activation relies on a balance of activating and inhibitory signals from receptors on their surface during the interaction with potential target cells. NK cells kill target cells through exocytosis of cytotoxic granules containing perforin and granzymes (4), induction of death receptor–mediated apoptosis (5), and antibody-dependent cellular cytotoxicity (6). In addition, NK cells secrete cytokines such as IFNγ, which activate other immune cells in their vicinity (7). In the context of cancer immunoediting, NK cells play a crucial role in eliminating tumor cells (8) and limiting their metastatic spread (9). NK cells spare healthy tissue and represent a safe treatment option with minimal risk of causing adverse effects (10). As a result, there is growing interest in using NK cells for immunotherapies, but to do this effectively, we require a better understanding of how tumor cells evade NK-cell attacks. Most studies to date have focused on the interaction between NK cells and tumor cell lines obtained from patients (11–16). These tumor cells have already successfully evaded the patient's immune system and may thus not represent suitable models to study immunoediting.

Here, we used an *in vitro* co-culture model based on non-edited NK cell–naïve mouse BCR/ABL^{p185+} B-cell acute lymphoblastic leukemia (B-ALL) cells to investigate the primary interaction of tumor and NK cells. NK cell–resistant tumor cells that emerged during the co-culture showed an upregulation of many IFNγ–dependent genes, such as lymphocyte antigen 6 complex, locus A (*Ly6a*). Further analysis identified Ly6A as a driver of NK cell–mediated immune evasion of mouse leukemia and extended our knowledge about the role of LY6E in limiting NK-cell antitumor activity. Moreover, we established a model to quantify NK-cell effector

[1]St. Anna Children's Cancer Research Institute (CCRI), Vienna, Austria. [2]Center for Physiology and Pharmacology, Institute of Pharmacology, Medical University of Vienna, Vienna, Austria. [3]Center for Physiology and Pharmacology, Department of Neurophysiology and Pharmacology, Medical University of Vienna, Vienna, Austria. [4]Division of Molecular Oncology & Immunology, Oncode Institute, Netherlands Cancer Institute, Amsterdam, the Netherlands. [5]Christian Doppler Laboratory for Next Generation CAR T Cells, Vienna, Austria. [6]Institut Curie, Université PSL, Sorbonne Université, CNRS UMR168, Laboratoire Physico Chimie Curie, Paris, France. [7]Biomedical Genomics, Biotechnology Center, Center for Molecular and Cellular Bioengineering, Technische Universität Dresden, Dresden, Germany. [8]Department of Hematology, Leiden University Medical Center, Leiden, the Netherlands. [9]Institute of Pharmacology, University of Veterinary Medicine Vienna, Vienna, Austria.

Corresponding Author: Eva M. Putz, Center for Physiology and Pharmacology, Institute of Pharmacology, Medical University of Vienna, Waehringer Strasse 13A, Vienna 1090, Austria. E-mail: eva-maria.putz@meduniwien.ac.at

Cancer Immunol Res 2025;13:430–46

doi: 10.1158/2326-6066.CIR-24-0189

functions and their ability to edit tumor cells by cellular DNA barcoding (17–19). In summary, this study shows that NK cells play a role in all three phases of cancer immunoediting and contribute to the active sculpting of tumor cells, ultimately driving tumor evasion.

Materials and Methods

Mice

C57BL/6JRj wild-type (WT) mice (RRID:MGI:2670020) were obtained from the Janvier Labs, and C57BL/6-Prf1^{tm1Sdz}/J (*Prf1*$^{-/-}$, strain #002407, RRID:IMSR_JAX:002407; ref. 20) and B6.129S7-Ifng^{tm1Ts}/J (*Ifng*$^{-/-}$, strain #002287, RRID:IMSR_JAX:002287; ref. 21) mice were obtained from the Jackson Laboratory. B6.129-B2m^{tm1Jae} (*B2m*$^{-/-}$, RRID:MGI:2175714; ref. 22) mice were kindly provided by Thomas Kolbe (University of Veterinary Medicine, Vienna). The mice were between 8 and 12 weeks of age and maintained under specific pathogen-free conditions according to the Federation of European Laboratory Animal Science Associations guidelines. Mice were used only for organ collection, and according to Austrian law, organ collection does not require the approval from an Institutional Animal Care and Use Committee.

Cell culture

Phoenix-ECO (ATCC, female, RRID:CVCL_H717) and Lenti-X 293T packaging cells (Takara, female, RRID:CVCL_1926) were cultured in DMEM medium (Thermo Fisher Scientific) with 10% FBS (Capricorn Scientific). The K562 cell line (ATCC, female, RRID:CVCL_0004) was cultured in RPMI medium (Gibco) supplemented with 100 U/mL penicillin and 100 μg/mL streptomycin (Gibco), 10% FBS, and 50 μmol/L β-mercaptoethanol (Sigma-Aldrich) (cRPMI). K562 cell authentication was conducted by Multiplexion in October 2020 and showed an identity of 100%.

To generate BCR/ABL^{P185+} cell lines, bone marrow (BM) was isolated from 8- to 10-week-old female and male mice, and single-cell suspensions were prepared through repeated homogenization using 18G and 24G needles. Forty-eight hours before the infection of BM cells, Phoenix-ECO cells were transfected with a retroviral MSCV-BCR/ABL^{P185} vector (kindly provided by Veronika Sexl, University of Veterinary Medicine, Vienna) mixed with PureFection Transfection Reagent (System Biosciences). The BM cells were transduced for 1 hour with the fresh viral supernatant in the presence of 10 μg/mL polybrene (Sigma-Aldrich) and 10 ng/mL recombinant murine IL7 (PeproTech). Transformed B-ALL cells were maintained in cRPMI medium until they were stable cell lines characterized by continuous growth and the homogenous expression of CD19, B220, and CD43 by flow cytometry (approximately 2 months).

All cell lines were tested every 2 to 3 months for their mycoplasma negativity using the PCR Mycoplasma Detection Kit (Applied Biological Materials). Cell lines were maintained in culture for a maximum of 3 months, after which a fresh batch of younger cells was thawed for the experiments. Cell growth and survival were measured using a CASY counter (OLS OMNI Life Science) or a CellDrop BF (DeNovix).

Primary mouse NK (mNK) cells were isolated from spleens using the negative selection EasySep Mouse NK-cell Isolation Kit (STEMCELL Technologies) or positive selection CD49b (DX5) MicroBeads kit (Miltenyi Biotec) and cultured in cRPMI supplemented with 5,000 U/mL recombinant human IL2 (rhIL2, Miltenyi Biotec). mNK cells were identified as single live mCD45.2$^+$mCD3$^-$NK1.1$^+$mCD335$^+$ cells by flow cytometry.

Human NK (hNK) cells were isolated from four healthy donors from leucocyte reduction chambers purchased from the Department of Transfusion Medicine and Cell Therapy of the Medical University of Vienna after obtaining written consent in accordance to the Declaration of Helsinki. The isolation kit RosetteSep Human NK-cell Enrichment Cocktail (STEMCELL Technologies) was utilized, and NK cells were cultured in NK MACS medium (Miltenyi Biotec) supplemented with 5% human serum (Capricorn Scientific) and 500 U/mL rhIL2. hNK cells were determined as single live hCD45$^+$hCD3$^-$CD56$^{bright\ or\ dim}$ cells by flow cytometry.

DNA barcoding

Generation of the lentiviral barcode library LG2.1

The BC1DS_lib oligo containing a 21-nt random barcode sequence (Supplementary Table S1) was PCR amplified (14 cycles: 10 sec 98°C, 30 sec 57°C, 20 sec 72°C) with Phusion polymerase [New England Biolabs (NEB)]. The PCR-amplified product was column purified (MinElute PCR cleanup kit, Qiagen) and subsequently digested with XhoI and AscI, followed by ligation into the 3′ UTR of the GFP cDNA sequence within the pRRL lentiviral vector (23), using the ElectroLigase kit (New England Biolabs). Electrocompetent ElectroMax Stbl4 bacteria (Invitrogen) were electroporated with 6 ng ligation product, and a small fraction of the transformed bacteria was plated on Luria–Bertani (LB) agar plates to determine transformation efficiency, whereas the remaining bacteria were grown overnight in 400 mL LB medium (VWR Life Science) supplemented with 100 μg/mL ampicillin (Sigma-Aldrich). DNA was extracted from the bacterial culture using the Maxiprep kit (Invitrogen). To determine the library's barcode diversity and distribution, barcodes were amplified with a three-step PCR reaction protocol (see "DNA barcode sequencing") in biological and technical duplicates and sequenced on a HiSeq 3000/4000 device (Illumina) with 64-bp single-end reads at the Biomedical Sequencing Facility (BSF) Vienna.

Barcoding of tumor cells

Lenti-X 293T cells were transfected with the LG2.1 barcode library and the two packaging plasmids p8.9QV and pVSVG (kindly provided by Ton N. Schumacher, Netherlands Cancer Institute, and Leiden University Medical Center; ref. 18) using the PureFection Transfection Reagent. Virus supernatant was harvested after 48 and 72 hours and concentrated with AMICON columns (Sigma-Aldrich). Approximately 2×10^5 B-ALL cells were spinfected with serially diluted viral supernatant for 90 minutes at 900 × *g*. The transduction rate (% GFP$^+$ cells) was measured by flow cytometry 3 days after transduction. Tumor cells with the desired transduction rate [<5% (17)] were expanded and FACS sorted to enrich for GFP$^+$ cells. Barcoded tumor cells were frozen for further experiments.

Flow cytometry

Cells were analyzed on a FACSymphony A3 Cell Analyzer device (Becton Dickinson, BD) and sorted on a FACSAria Fusion device (BD). The antibodies and cell stains used in this study are listed in Supplementary Table S2. The acquired data were analyzed with the FlowJo v10 software. Single living cells were gated according to size and granularity in FSC-A, SSC-A, and FSC-H plots, and cell surface marker expression was quantified by median fluorescence intensity (MFI). Gating strategies and representative plots are shown in Supplementary Figs. S1–S3.

In vitro co-culture system and tumor cell growth analysis

Approximately 9×10^5 barcoded B-ALL cells were co-cultured with mNK cells (4 days after isolation) in an effector-to-target (E:T) ratio of 1:1 in three biological replicates per condition. Depending on NK cell–mediated cytotoxicity and tumor cell growth, cells were harvested for FACS sorting and further analyses on days 4 to 6 and 14 to 17. On the day of harvesting, 3×10^5 tumor cells were co-cultured for a second or third time with 4-day-old mNK cells (E:T = 1:1). All conditions were cultured in the presence of 2,500 U/mL rhIL2. Wherever indicated, tumor cells were treated with 2 ng/mL mouse IFNγ (Abcam) every 2 to 3 days. During the co-culture, the absolute number of B-ALL tumor cells was determined by flow cytometry using AccuCheck Counting Beads (Invitrogen). Tumor cells were identified by gating on single live $mCD45.2^+mCD19^+GFP^+$ cells.

Cytotoxicity assay

Approximately 5×10^4 CellTrace Violet (CTV, Invitrogen)-stained B-ALL or K562 cells were seeded in 96-well round-bottom plates and IL2-activated mNK or hNK cells were added in the indicated E:T ratios in technical duplicates or triplicates. After 1 hour or 4 hours of incubation at 37°C, cells were stained with fixable viability dye eFluor 780 (Invitrogen) and fixed with fixation buffer (BioLegend) before flow cytometric analysis. The percentage of specific NK-cell lysis was calculated as follows: (% dead tumor cells after co-incubation with NK cells − % spontaneous lysis)/(100% − % spontaneous lysis).

Effector function assay

Approximately 5×10^4 CTV^+ B-ALL or K562 cells were cultured with 5×10^4 IL2–activated mNK or hNK cells, respectively. As positive control, we used mNK or hNK cells stimulated with cell stimulation cocktail (Invitrogen) or 10 ng/mL IL12 (PeproTech) + 100 ng/mL IL15 (PeproTech) + 15 ng/mL IL18 (R&D System), respectively. One hour after the start of co-culture, Brefeldin A (BioLegend) was added, and 3 hours later cells were stained with fixable viability dye eFluor 780, fixed with fixation buffer and permeabilized with intracellular staining permeabilization wash buffer (BioLegend) before the intracellular staining of the cells for IFNγ, granzyme B, and TNFα.

Conjugation assay

Tumor cells were stained with CTV, and NK cells were either stained with anti-mNK1.1 or anti-hCD56. An equal number of tumor and NK cells were added into a FACS tube, and cells were centrifuged for 3 minutes at $100 \times g$. After no (human) or 10 minutes (mouse) incubation at 37°C, cells were vortexed for 3 seconds and fixed with ice-cold 0.5% paraformaldehyde (Electron Microscopy Sciences) in PBS. Cells were kept on ice and immediately measured by flow cytometry. Living cells were gated according to size and granularity in FSC-A and SSC-A plots, doublets were included in the analysis, and CTV and CD56 or NK1.1 double-positive tumor–NK-cell conjugates were quantified.

Multiomics approaches

Approximately 10^6 GFP^+ barcoded tumor cells were FACS sorted, washed twice with PBS, and snap frozen. DNA and RNA were extracted using the AllPrep DNA/RNA Mini Kit (Qiagen).

DNA barcode sequencing

Library preparation for barcode sequencing was performed in technical duplicates with three nested PCR steps. PCR#1 amplified the barcodes, PCR#2 added the required sequences for the universal Illumina adapters and four random base pairs (bps) for a more diverse sequencing start, and PCR#3 attached the P5 and P7 universal Illumina adapters and with the P7 a sample–specific index sequence (primer sequences and reagents are in Supplementary Table S1). The samples were cleaned up with Agencourt AMPure XP beads (Beckman Coulter). Up to 96 equimolar pooled samples spiked with 10% to 15% PhiX (Illumina) were sequenced with the MiSeq Reagent Kit v3 (150 cycles; Illumina) 64-bp single-end reads with a coverage of 50 to 100 reads/barcode.

Barcode/cell clone evolution analysis

The R statistics software (RRID:SCR_001905, v4.0.3) was used to analyze barcode abundance and clonal diversity. Unmapped reads were loaded from FASTQ format (function "readDNAStringSet" from package Biostrings v2.58.0, RRID:SCR_016949) into the R environment. Barcode sequences were located by pattern matching (function "vmatchPattern" from package Biostrings) to identify the fixed head ("GAACACTCGAGATCAG") and non-variable ("TGTGGTATGATGT") portions of the reads, which enclose the barcodes from left and right, respectively. Sequences that did not meet the expected length (21 bases) or included uncalled bases ("N") were discarded (mean discarded sequences = 15%). To define the barcodes of the reference library, we selected sequences with a sum of at least 100 reads across samples ($n = 4$) of the viral library for further analysis. With these we constructed a count matrix indicating the number of reads matching each barcode. Technical replicates were merged by adding up the read counts. For each cell line, only barcodes detected across three B-ALL-alone samples at the corresponding reference time point with a total sum of at least nine reads were considered for downstream analysis. Barcode diversity for each sample was quantified using Shannon diversity as follows: $sum(p * \log(p), \text{na.rm} = \text{TRUE}) * -1$, in which p is the ratio of the counts of each barcode relative to the total barcode counts. Shifted $\log_2$ transformation was used for normalization (function "normTransform" from package DESeq2, RRID:SCR_015687, v1.30.0). Based on the statistics of differential abundance and variability across samples [here, the variability was calculated as following: $v = log2(max(x+1)/min(x+1))$, in which x is a vector of normalized counts across samples] at every time point, barcodes were assigned to one of five categories: (i) primary resistant: differentially abundant (P adj <0.05) and increasing [$\log_2$(fold change) ≥1; comparing B-ALL + NK vs. B-ALL alone]; (ii) eliminated: differentially abundant (P adj <0.05) and decreasing [$\log_2$(fold change) ≤ −1; comparing B-ALL + NK vs. B-ALL alone]; (iii) static: variability $v \leq 0.5$ in B-ALL alone and $v < 1$ at B-ALL + NK; (iv) secondary resistant: low variability $v \leq 0.5$ in B-ALL alone, high variability in B-ALL + NK $v \geq 1$, and barcode abundance high in only one of the three replicates; and (v) others: none of the above. Barcodes were further ordered using hierarchical clustering (function "hclust" from package *stats* v4.0.3, method = "ward.d2," RRID:SCR_014673). Heatmaps were generated using ComplexHeatmap (RRID:SCR_017270, v2.7.5.1), and bubble plots were generated using MATLAB (RRID:SCR_001622).

RNA sequencing

After RNA isolation, samples were treated with DNase I (Thermo Fisher Scientific). Library preparation and sequencing were performed at the BSF of the Research Center for Molecular Medicine (CeMM) of the Austrian Academy of Sciences. RNA sequencing (RNA-seq) libraries were prepared with the QuantSeq 3′ mRNA-Seq Library Prep Kit (FWD) for Illumina (Lexogen). For sequencing, samples were pooled into NGS libraries in equimolar amounts. Expression profiling libraries were sequenced on HiSeq 3000/4000 or NovaSeq 6000 instruments (Illumina) following a 50-, 100-, or 120-base-pair single-end setup. Raw data acquisition and base calling were performed on-instrument, whereas the subsequent raw data processing

off the instruments involved two custom programs based on Picard tools (RRID:SCR_006525, v2.19.2). In a first step, base calls were converted into lane–specific, multiplexed, unaligned BAM files suitable for long-term archival (IlluminaBasecallsToMultiplexSam, 2.19.2-CeMM). In a second step, archive BAM files were demultiplexed into sample–specific, unaligned BAM files (IlluminaSamDemux, 2.19.2-CeMM).

RNA-seq analysis

Mapping of the reads was performed using STAR (RRID:SCR_004463, v2.7.10a; ref. 24) to the *Mus musculus* GRCm38 or *Homo sapiens* GRCh38 assemblies, and duplicate reads were identified with Picard (v2.27.4). Quantification of the mapped reads was carried out using Salmon (RRID:SCR_017036, v1.8.0; ref. 25). The following data processing and visualization were performed in R (v4.2.0). To ensure robustness of the analysis, the dataset was filtered to include only transcripts detected in at least three samples. The analyses of mouse cell lines A and B and cell lines C and D were performed separately. Finally, the results were compared.

For count normalization, variance stabilization, and differential expression analysis, the Bioconductor DESeq2 (v1.38.3) package was used. DESeq2 employs a negative binomial distribution-based model, with additional shrinkage using apeglm (26) or ashr algorithms (v1.20.0). Transcripts were considered significantly differentially expressed between groups if they exhibited a $\log_2$(fold change) $\geq$0.58 and a P adj $\leq$0.05.

The principal component analysis (PCA), expression heatmaps, and volcano plots were generated using ggplot2 (v3.4.2) and heatmap (v1.0.12). To correct for batch effects between different experiments in PCA plots, the limma R (27) package (RRID:SCR_010943, v3.54.2) was utilized. The resulting gene lists were annotated and subjected to gene set enrichment analysis (GSEA, RRID:SCR_003199). Visualization of the GSEA results was achieved using the hypeR (28) package (v2.0.1) and represented as dot plot. Gene Ontology Biological Process terms were obtained from the Molecular Signatures Database (MSigDB) using the msigdbr (29) package (RRID:SCR_016863, v7.5.1).

Assay for transposase-accessible chromatin sequencing (ATAC-seq)

Approximately 5×10^4 GFP^+ tumor cells were FACS sorted into 1.5 mL microcentrifuge tubes containing 400 µL 0.5% bovine serum albumin (BSA, GE Healthcare) in PBS and pelleted. Cells were lysed, and the DNA was tagmented for 30 minutes at 37°C using 25 µL tagment DNA enzyme in tagment DNA buffer (Illumina), 1% digitonin (Promega), and EDTA-free protease inhibitor cocktail (Roche). Samples were purified with the Qiagen MinElute kit (Qiagen). Libraries were generated as described by Buenrostro and colleagues (30) by using the Ad1_noMx and Ad2.1-Ad2.48 indexed primers (Supplementary Table S1). PCR products were purified with Agencourt AMPure XP beads, and the sample profile was analyzed with the High Sensitivity D5000 kit (Agilent Technologies) on a TapeStation (Agilent Technologies). Approximately 45 to 48 equimolar pooled samples were sequenced on a NovaSeq 6000 instrument with 50-bp paired-end reads at the BSF (CeMM).

ATAC-seq analysis

The obtained raw reads were processed using the ATAC-seq Nextflow (31) pipeline (v2.0). This included mapping the reads with STAR to the GRCm38 genome, identification of duplicates with Picard (v2.27.4), and calling broad peaks with MACS2 (bioRxiv 2018.496521; v2.2.7.1). Peaks overlapping with blacklisted (GRCh38) regions were filtered out, and the remaining peaks were annotated with HOMER (RRID:SCR_010881, v4.11; ref. 32). Consensus peaks across all samples were identified with BEDTools (RRID:SCR_006646, v2.30.0; ref. 33), and counting reads in these peaks was done with featureCounts (RRID:SCR_012919, Rsubread v2.0.1; ref. 34). Visualization of the ATAC-seq peaks was performed by creating BigWig files with bedGraphToBigWig (v377) and exporting to the Integrative Genomics Viewer browser (RRID:SCR_011793, v2.16.1; ref. 35). Quality of the obtained raw data was assessed with MultiQC (RRID:SCR_014982, v1.13; ref. 36). Data processing and visualization were performed in R (v4.2.0). To ensure robustness of the analysis, the dataset was filtered to include only consensus peaks detected in all three replicates of each condition and cell line and only the peaks that were located in the window of ±3 kb around the transcription start site. The analysis of cell lines A and B was performed separately from the analysis of cell lines C and D.

Similar to the RNA-seq analysis, the Bioconductor DESeq2 (1.38.3) package was used for count normalization, variance stabilization, and analysis of differential accessibility. Peaks were considered significantly accessible between groups of comparison if they exhibited a $\log_2$(fold change) $\geq$0.58 and a P adj $\leq$0.05. Exploratory analysis included PCA, production of heatmaps, volcano plots, and GSEA.

Integration of RNA-seq and ATAC-seq data

To integrate two datasets and perform genome-wide quantification of differential transcription factor (TF) activity in cell lines at different time points, we used diffTF (v1.8; ref. 37). The processing was done only for A and B datasets because of very high computational demand of the algorithm. The input consisted of raw ATAC-seq reads in BAM files, filtered consensus peaks from the previous step, raw RNA-seq counts, and positional weight matrix (PWM) data for all TFs: HOCOMOCO (RRID:SCR_005409, v10; ref. 38).

2D reversed-phase/reversed-phase liquid chromatography/tandem mass spectrometry analysis

Cells were lysed in 200 µL lysis buffer (50 mmol/L HEPES pH 8.0, 2% SDS, 1 mmol/L PMSF, cOmplete Protease Inhibitor Cocktail, Roche) and heated to 99°C for 5 minutes, and DNA was sheared using a Covaris S2 ultrasonicator. Lysates were cleared at 20,000 × g for 15 minutes at 20°C, and tryptic digest was performed using filter-aided sample preparation according to Wisniewski and colleagues (39). Peptides were desalted (C18 solid-phase extraction; Pierce Peptide Desalting Columns, Thermo Fisher Scientific), labeled with TMTpro 16plex reagents (Thermo Fisher Scientific), pooled, dried in a vacuum concentrator, and cleaned up via C18 solid-phase extraction. After re-buffering in 10 mmol/L ammonium formate buffer pH 10, peptides were fractionated via a C18 column (150 × 2.0 mm Gemini-NX, 3 µm, C18 110 Å, Phenomenex) on a Dionex UltiMate 3000 nanoLC (Thermo Fisher Scientific). Fractions were dried in a vacuum concentrator and taken up in 0.1% TFA before analysis.

Mass spectrometry analysis was performed on an Orbitrap Fusion Lumos Tribrid Mass Spectrometer coupled to a Dionex UltiMate 3000 nanoLC system via a Nanospray Flex Ion Source interface (all from Thermo Fisher Scientific) using the same procedure as Block and colleagues (40). Data analysis was performed using the Proteome Discoverer platform (RRID:SCR_014477, v.2.4.1.15).

Genome editing

Ribonucleoprotein–mediated CRISPR genome editing of B-ALL cells

Cells were transfected with crRNAs, Alt-R CRISPR Cas9 tracrRNA ATTO 550, and Alt-R S.p. Cas9-GFP V3 (all IDT) with

the Gene Pulser Xcell electroporation system (Bio-Rad) using the following settings: 350 V, 5 ms, and 1 pulse. The crRNA sequences were as follows: *Ly6a*: TCACGTTGACCTTAGTACCC; TATTGAAAGTATGGAGATCC, and *Plaat3*: CGTCATGTTTGTTATTGACC; ATGGCCCAGTGTCTGTACAT. The next day, $GFP^+ATTO\ 550^+$ tumor cells were single-cell FACS sorted into 96-well flat-bottom plates into 50% tumor cell–conditioned medium and 50% fresh cRPMI. After the outgrowth of single clones, the KO was validated by Tracking of Indels by DEcomposition (TIDE) sequencing. Up to 2×10^5 cells were lysed in 50 μL Pawel's buffer at 56°C for 15 minutes with subsequent heat inactivation at 95°C for 5 minutes. After centrifugation at 2,000 × *g* for 5 minutes, the supernatant was used for the TIDE PCR to amplify the breakpoints of the guide RNAs (primer sequences and reagents in Supplementary Table S1). PCR products were Sanger sequenced (Microsynth) and analyzed for their genotype with the TIDE (nki.nl) web tool (RRID:SCR_023704). Gene knockouts were validated using flow cytometry or quantitative PCR.

CRISPR genome editing in Cas9–expressing K562 cell line

K562 were transduced to express Cas9 with lentiviral supernatant from Lenti-X 293T cells 48 hours after transfection with the following constructs: lentiCRISPRv2 (RRID:Addgene_52961), p8.9QV, and VSV-G. K562 cells were transduced by spinfection for 90 minutes at 900 × *g*. Transduced cells were selected with 1 μg/mL puromycin (Sigma-Aldrich) for up to 7 days. crRNA specific for *LY6E* (GTGACTGTGTCTGCTAGTGC) was transfected into K562-Cas9 cells with the Gene Pulser Xcell electroporation system using the following settings: 400 V, 3 ms, and 1 pulse. The cells were single-cell FACS sorted into 96-well flat-bottom plates into 50% 48-hour-old medium of tumor cells and 50% fresh cRPMI with 100-gray irradiated K562-mbIl15-41-BBL (RRID:CVCL_C7IM, kindly provided by Manfred Lehner, CCRI and Christian Doppler Laboratory for Next Generation CAR T Cells, Vienna). After the outgrowth of single clones, the KO was validated by TIDE sequencing (primer sequences in Supplementary Table S1) and immunoblotting.

Quantitative PCR

To validate the *Plaat3* deficiency in B-ALL cells, RNA was extracted from 2×10^6 cells with the Monarch Total RNA Miniprep Kit with "on column" DNase I treatment (NEB). cDNA was generated from 1 μg RNA by using the LunaScript RT SuperMix Kit (NEB), and qPCR was performed with the Luna universal qPCR Master Mix (NEB) using 1 μL cDNA template in technical duplicates and two independent experiments (primer sequences in Supplementary Table S1). The qPCR was conducted on a 7500 Real-Time PCR System device (Applied Biosciences), and the data were analyzed with the 7500 Software (RRID:SCR_014596, v2.0.6). The housekeeping gene *Gapdh* was used for normalization, and the relative expression values of *Plaat3* were calculated by the $2^{-\Delta CT}$ method.

Immunoblotting

To analyze LY6E protein expression, *LY6E* WT and KO cells were cultured with or without 10,000 U/mL IFNβ (Miltenyi Biotec) or 10 ng/mL IFNγ (PeproTech) overnight. Cells were lysed in RIPA buffer (Sigma-Aldrich) with protease inhibitor cocktail (Thermo Scientific) and phosphatase inhibitor cocktail II (Abcam). Equal amounts of protein were separated on an SDS polyacrylamide gel. Proteins were transferred to a nitrocellulose membrane by using the Trans-Blot turbo transfer kit and system (Bio-Rad). After blocking in 5% BSA-TBS-T, membranes were probed with primary antibodies against LY6E (Invitrogen) and β-actin (Cell Signaling Technologies) overnight, before the staining with a fluorescent secondary antibody (Thermo Scientific) and visualization by the ChemiDoc MP imaging system (Bio-Rad). See Supplementary Table S2 for antibody details.

Seahorse—ATP rate assay

Approximately 3.5×10^4 *Ly6a* WT or KO cells were seeded in triplicates into the Seahorse XF HS PDL Miniplates (Agilent) and centrifuged at 300 × *g* for 2 minutes. The assay was conducted according to manufacturer's protocol, measured on the Agilent Seahorse XF HS Mini Analyzer (Agilent), and analyzed with the online Agilent Seahorse Analytics software.

IFNγ ELISA

Tumor cells were split to 3×10^5 cells/mL on day 0 and cultivated for 48 hours in cRPMI. On day 2, the supernatant was harvested, filtered through a 45 μm filter, and transferred onto IL2-expanded mNK cells in the presence of 2,500 U/mL rhIL2. After 48 hours, mNK cells were harvested and the supernatant was frozen at −80°C. For a positive control, we stimulated mNK cells with cell stimulation cocktail (Invitrogen) 4 hours before the supernatant harvesting. The ELISA was performed according to the manufacturer's protocol (Abcam, ab100690) and analyzed using the web tool https://www.arigobio.com/elisa-analysis.

Statistical analysis

Statistical analysis was performed using GraphPad Prism (RRID:SCR_002798, v8.4.3 for Windows) using two-tailed paired and unpaired *t* tests, one-way or two-way ANOVA, or Kruskal–Wallis tests as indicated. When ANOVA showed a statistical difference, Tukey's multiple comparison testing or Dunnett's *post hoc* testing was applied. The α-level for all tests was set to 0.05, and *P* values were two-tailed. The significance level is indicated as follows: *, $P < 0.05$; **, $P < 0.01$; ***, $P < 0.001$; ****, $P < 0.0001$.

To generate the heatmaps in **Fig. 1** and Supplementary Fig. S4, the data were pooled from two to four independent experiments by calculating the mean surface marker expression or mean % specific lysis at E:T ratio of 10:1. The values were standardized for each variable (row) using the following calculation: *Z*-score = (mean of observed values − mean of the samples)/(standard deviation of the samples). The heatmaps were generated using the ClustVis web tool (41).

Heatmaps in other figures were generated by using the R package ComplexHeatmap (v2.10.0). The raw MFI values minus the MFI of their unstained control served as input. Rows (surface markers) were scaled and clustered (unsupervised). Columns (cell lines) were ordered by genotype and cell line.

Data availability

Data generated in this study are publicly available in Gene Expression Omnibus at GSE278011 (DNA barcode sequencing), GSE278010 (ATAC sequencing), and GSE278006 (RNA sequencing). The computer codes for the data analysis are available on GitHub (https://github.com/TumorImmunoEditingLab). All other data are available in the manuscript and its associated supplementary files.

Results

Quantitative measure of NK-cell effector functions

As a model to study leukemic tumor cell evasion from NK cells, we established a long-term *in vitro* co-culture system using IL2-activated primary mNK cells co-incubated with NK cell–naïve DNA-barcoded B-ALL cell lines for up to 20 days (**Fig. 1A**). We generated several independent B-ALL cell lines from the BM of WT ($n = 10$) and MHC-I–deficient mice ($B2m^{-/-}$, $n = 10$) and

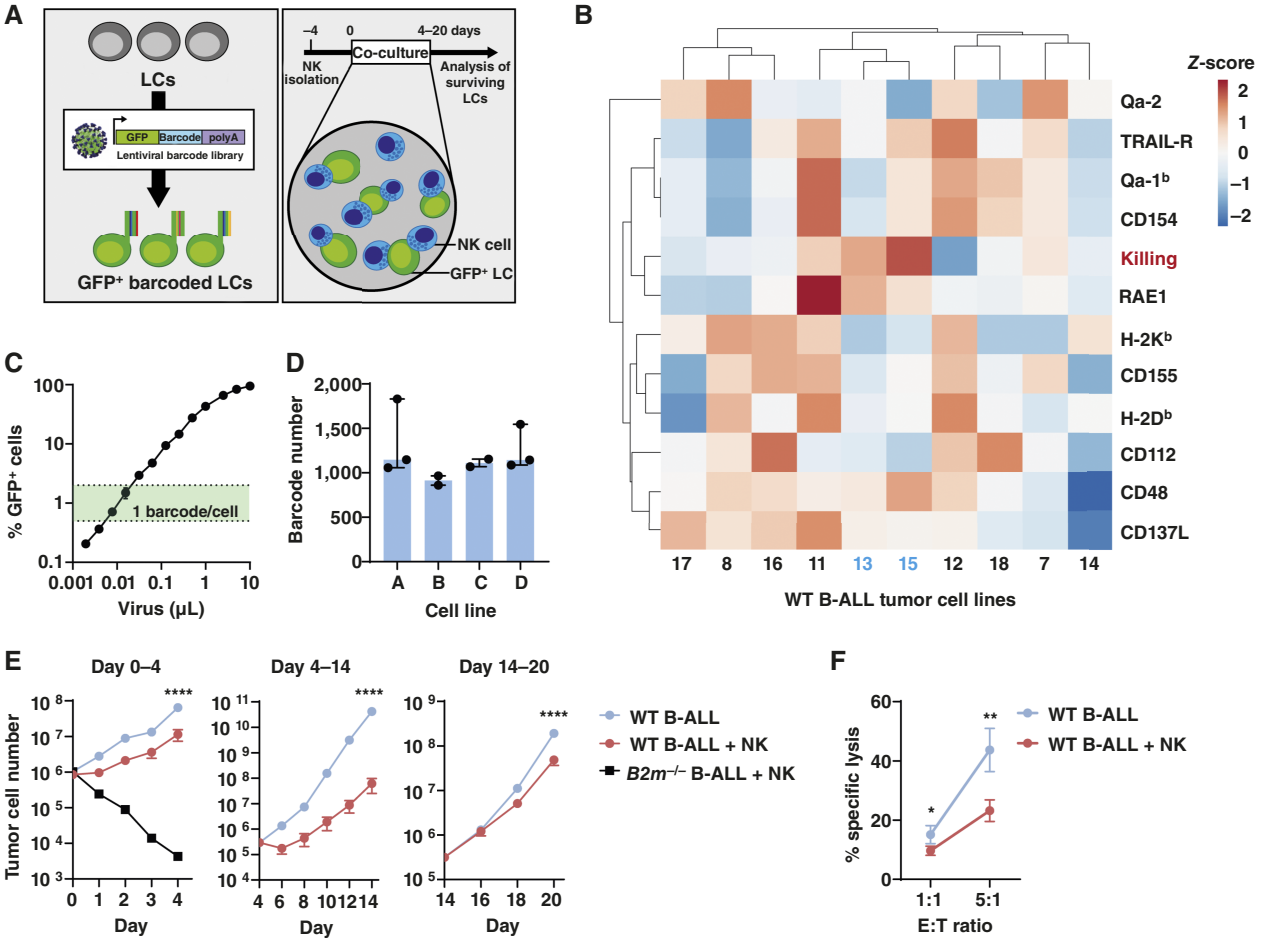

Figure 1.

Co-culture system to study cancer immunoediting *in vitro*. **A,** Scheme illustrates the experimental setup: BCR/ABL^{p185+} B-ALL leukemic cells were transduced with a DNA barcode library. Barcoded leukemic cells were co-cultured with NK cells for 4 to 20 days *in vitro*. **B,** Ten B-ALL cell lines were generated from C57BL/6 WT mice and characterized regarding the surface expression of NK cell–receptor ligands (black) and their susceptibility toward NK-cell killing (red, depicted here is the cytotoxicity at E:T ratio of 10:1) measured by flow cytometry. Shown is the summary of two independent experiments. Cell lines #13 and #15, in blue, showed the highest NK-cell susceptibility and were used for the following experiments. Rows were centered; unit variance scaling was applied to rows. Both rows and columns were clustered using correlation distance and average linkage. **C,** B-ALL cell lines were DNA barcoded by lentiviral transduction. Using different amounts of viral supernatant, the optimum transduction efficiency of <5% GFP$^+$ cells (17) was chosen to allow a single barcode integration per cell. Shown are means ± SD ($n = 2$) of one cell line. **D,** Two B-ALL cell lines (#13 and #15) were barcoded, and the barcode diversity of the FACS-purified GFP$^+$ cell lines was determined by targeted DNA sequencing. Cell lines A and B were derived from #13 and cell lines C and D from #15. Bars show barcode diversity of barcoded tumor cell lines (A and D, $n = 3$; and B and C, $n = 2$ independent experiments, each determined by sequencing of three biological and two technical replicates). Shown is the median with interquartile range. **E,** Barcoded WT B-ALL cell lines A–D were cultivated in three individual wells either in the absence or presence of purified and IL2-activated NK cells. One *B2m*$^{-/-}$ B-ALL cell line was included as positive control for NK-cell killing. Absolute numbers of B-ALL cells were determined by flow cytometry. On days 0, 4, and 14, B-ALL cells were FACS sorted and replated, and fresh NK cells were replenished. Shown are means ± SD of $n = 4$ B-ALL cell lines of one representative experiment ($n = 3$ independent experiments); the significance was calculated by an unpaired *t* test on days 4, 14, and 20. **F,** On day 29, a 4-hour NK cytotoxicity assay was performed using B-ALL cells that had been cultured for 20 days in the presence or absence of NK cells. Shown are means ± SD of $n = 4$ cell lines (in technical triplicates) of one representative experiment ($n = 3$ experiments); the significance was calculated by a paired *t* test. *, $P < 0.05$; **, $P < 0.01$; ****, $P < 0.0001$. LCs, leukemic cells.

characterized their surface expression of ligands for NK-cell receptors and susceptibility to NK cell–mediated killing. The two WT cell lines that showed the highest susceptibility toward NK cells (#13 and #15) expressed enhanced levels of the activating NKG2D-ligand RAE1 and lower levels of inhibitory ligands (e.g., classical and nonclassical MHC-I proteins H2-K^b, H2-D^b, Qa-1^b, and Qa-2; **Fig. 1B**). *B2m*$^{-/-}$ B-ALL cell lines showed a higher susceptibility toward NK cells according to the recognition of missing self (Supplementary Fig. S4A; ref. 42). To allow for a systematic quantification of NK-cell effector functions, a DNA barcode library was introduced into the WT B-ALL cell lines #13 and #15 ($n = 2$ each) to track individual tumor cell clones over time. For this purpose, a new lentiviral barcode library (LG2.1, containing 52,645 barcodes) was generated consisting of 21 random nucleotides positioned downstream of a *GFP* gene (Supplementary Fig. S4B–S4E). The lentiviral library was introduced into the B-ALL cell lines at a low multiplicity of infection to ensure the integration of a single barcode per cell (**Fig. 1C**; refs. 17, 43). To enrich for barcoded cells, GFP$^+$ cells were FACS sorted shortly after transduction and before the long-term co-culture with NK cells. The barcode diversity of the resulting four cell lines called A and B (derived from #13)

and C and D (derived from #15) was determined by site–specific PCR amplification and next-generation sequencing (**Fig. 1D**). The barcoded cells were co-incubated with NK cells at an E:T ratio of 1:1. After 4 and 14 days, GFP^+ tumor cells were FACS purified and fresh NK cells were replenished to rechallenge the tumor cells. Throughout the experiment, the absolute number of GFP^+ tumor cells was determined by flow cytometric analysis (**Fig. 1E**). Although the tumor cells showed significantly slower proliferation in the presence of NK cells during the first two rounds of co-culture, this difference became marginal in the third round. Twenty-nine days after the start of co-culture, we performed a cytotoxicity assay. The extended co-culture of leukemic cells with NK cells induced resistance toward NK cell–mediated killing and led to tumor evasion of the NK cells *in vitro* (**Fig. 1F**).

NK cell–mediated editing of leukemic cells

There are four conceivable fates of B-ALL tumor cell clones upon long-term co-culture with NK cells: The abundance of a clone could be lower ("eliminated"), higher ("primary resistant"), unchanged ("static"), or highly variable ("secondary resistant"; **Fig. 2A**). After bulk DNA sequencing of the barcodes, we designed a decision tree to discriminate these four categories algorithmically (**Fig. 2B**). Primary resistance, also known as intrinsic resistance (44), is defined as *a priori* resistance toward therapy. In our study, primary resistance was characterized by a reproducible and significant accumulation of a clone despite the presence of NK cells in co-culture. In comparison, secondary resistance describes the phenomenon of acquired resistance, represented by a situation in which a tumor can initially respond effectively to therapy but relapse or progress after treatment (45). We hypothesized that secondary resistance was not a general tumor-intrinsic property but acquired only by a subfraction of sibling cells and would therefore be observed only in isolated wells (**Fig. 2A**). Indeed, clustering of the barcoded leukemic cells according to the predefined categories (**Fig. 2C** and **D**) showed that most clones were efficiently eliminated (mean ± SD = 58.5 ± 4.8%, n = 2–3 independent experiments, n = 2–4 B-ALL cell lines). A smaller number of cell clones showed an NK cell–resistant phenotype (14.3% ± 4%) or remained static (23.9% ± 4.4%) despite the presence of NK cells. As hypothesized, we also observed secondary resistance, characterized by the presence of a cell clone in only one of the three replicate wells (3.3% ± 2.5%, **Fig. 2E**). In line with the paradigm that the acquisition of a resistant phenotype in tumor cells takes time, we observed the emergence of secondary resistance primarily at the later of the two sampling time points (Supplementary Fig. S5A). To be able to draw conclusions about the preexisting fate of the tumor cell clones, we compared two independent experiments with the same barcoded cell lines. As shown in **Fig. 2F** and Supplementary Fig. S5B, the cell clones attributed to the clusters primary resistant and eliminated had the same fate in both experiments. In contrast, the pool of secondary resistant tumor cell clones was distinctive for independent experiments. In summary, whereas primary resistant and eliminated cells harbored tumor-intrinsic properties *a priori* that determined their destiny, the fate of secondary resistant tumor cell clones was stochastic. This underscored our hypothesis that secondary resistant tumor cells acquired their resistant phenotype during co-culture with NK cells. Thus, our data showed that apart from direct killing, NK cells participated in immunoediting by actively shaping the tumorigenicity of individual tumor cells.

Molecular changes observed in NK cell–resistant B-ALL cells

To identify drivers of NK-cell resistance, we investigated the changes in the transcriptomic and chromatin accessibility profiles of NK cell–resistant B-ALL cells generated during the long-term *in vitro* co-culture. To this end, we performed RNA (**Fig. 3A–D**; Supplementary Fig. S6) and ATAC sequencing (**Fig. 3E** and **F**; Supplementary Fig. S7) and compared NK cell–co-cultured to NK cell–naïve tumor cells. The transcriptomic analysis showed a significant upregulation of genes with a well-known link to NK-cell evasion such as components of the MHC-I machinery [e.g., *Stat1*, *B2m*, *Tap1*, and *H2-K1* (46); **Fig. 3A**; Supplementary Fig. S6C]. Additionally, this analysis revealed a set of genes that included potential drivers of resistance to NK cells, such as *Ly6a* and phospholipase A and acyltransferase 3 (*Plaat3*). The functional enrichment analysis showed that the main biological process associated with the differentially expressed genes (DEGs) was the response to IFNγ (e.g., *Stat1*, *Irf1*, *Ccl5*, and *Cd74*; **Fig. 3B**), which is produced by activated NK cells in co-culture. After integrating the results from the four barcoded cell lines A–D, we observed that many DEGs upon NK-cell co-culture were cell line specific (up: A/B = 193 and C/D = 99, down: A/B: 211 and C/D = 63). However, a total of 129 genes were upregulated and 27 were downregulated in all four cell lines and may be universally associated with or driving escape from NK cells (**Fig. 3C**). The top 30 DEGs are depicted in the heatmap in **Fig. 3D**. Consistent with these data, the ATAC sequencing results showed the opening of chromatin at the promoters of classical IFN-inducible genes (e.g., *Iigp1*, *Ifi27*, *Mx1*), as well as of *Ly6a* and *Plaat3* (**Fig. 3E**; Supplementary Fig. S7C). We considered overlapping differentially accessible regions in cell lines A/B and C/D as the most robust ones (**Fig. 3F**). Integration of RNA and ATAC sequencing data by comparing the DEGs and differentially accessible regions in cell lines A/B showed a significant intersection (37 genes up/open, 16 genes down/closed). The two highly upregulated genes *Ly6a* and *Plaat3* in the transcriptomic analysis were also present in this strictly filtered dataset (**Fig. 3G**). The quantification of differential TF activity by integrating the RNA and ATAC sequencing datasets revealed TFs involved in resistance to NK cells. We classified TFs as activators (NF2L1, SMRC1, JUN, IRF1, and IRF9) or repressors (RXRB and JUND), based on their expression and accessibility of predicted binding sites (37). STAT1 expression was clearly upregulated as the major TF downstream of IFNγ signaling, but it showed activating and repressive functions and was therefore classified as undetermined (**Fig. 3H**). A closer look at the top hits *Ly6a* and *Plaat3* showed that both have multiple predicted binding sites for STAT1, IRF1, and IRF9 based on the occurrence of DNA sequence motifs in the vicinity of accessible chromatin (**Fig. 3I**). In summary, multiomics analyses revealed that the B-ALL cells that were not *a priori* sensitive and eliminated by NK cells showed a highly NK cell–resistant phenotype characterized by a strong IFNγ signature and the upregulation of *Ly6a* and *Plaat3*.

Relative contribution of NK-cell cytotoxicity and IFNγ production in cancer immunoediting

The two main functions of NK cells are the direct lysis of tumor cells and the production of proapoptotic and proinflammatory cytokines, most importantly IFNγ. To discriminate the relative contributions of killing and cytokine production to cancer immunoediting, we performed two independent long-term co-culture experiments with NK cells deficient in perforin ($Prf1^{-/-}$), which renders them unable to kill their target cell (20), or deficient in IFNγ production ($Ifng^{-/-}$; **Fig. 4**; Supplementary Figs. S8 and S9; ref. 21). As described above, the growth of GFP^+ tumor cells was measured by flow cytometry during the experiment. On days 4 and 14 (for $Prf1^{-/-}$) or on days 4 and 17 (for $Ifng^{-/-}$), GFP^+ tumor cells were sorted and

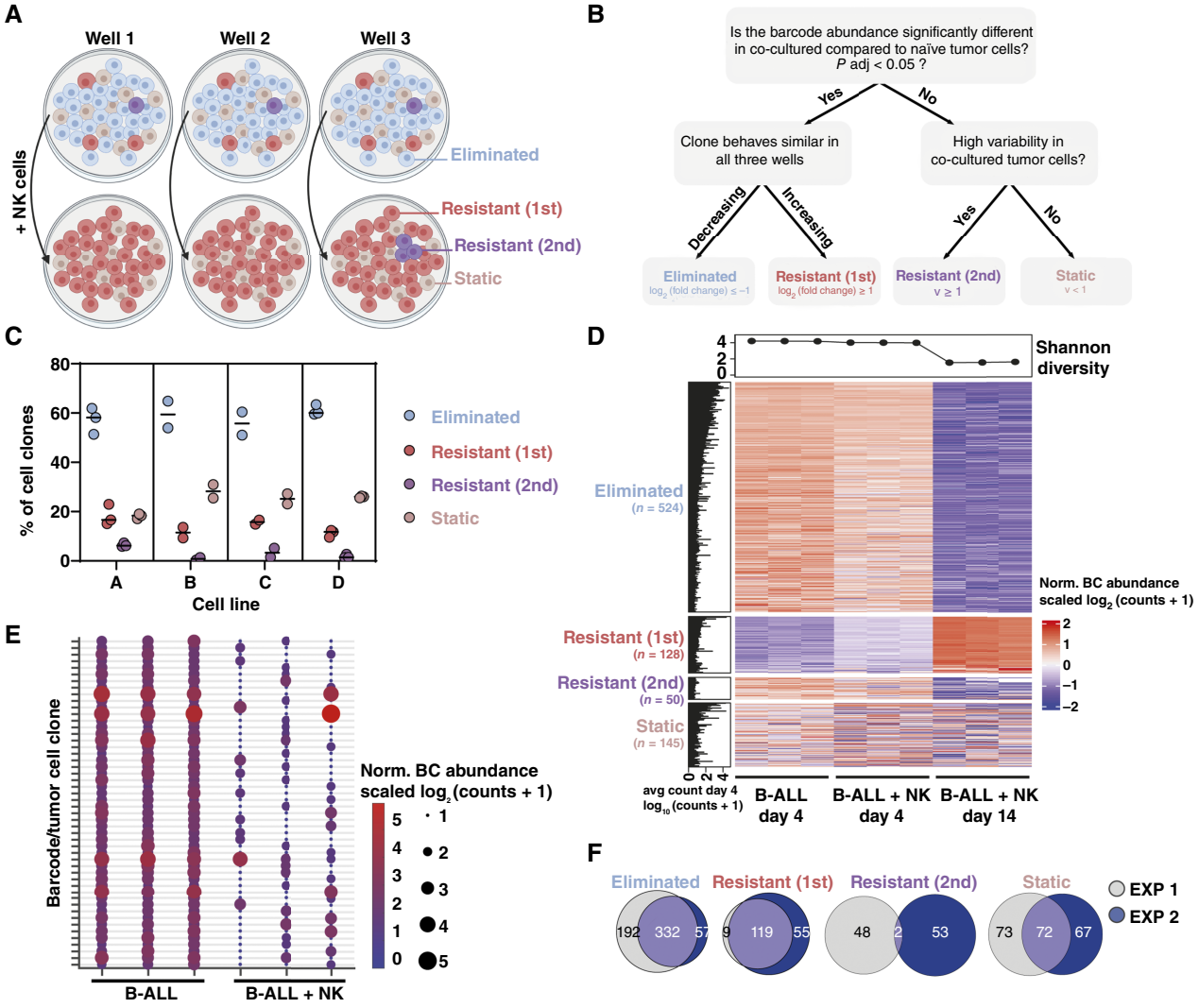

Figure 2.

Quantification of NK cell–mediated cancer immunoediting *in vitro*. **A,** Schematic representation of the proposed model. **B,** Upon long-term co-culture of B-ALL and NK cells, we hypothesized that each tumor cell clone would fall into one of the following categories: the abundance of a clone can be significantly higher [primary resistant (1st)], lower (eliminated), unchanged (static), or show a high variability [secondary resistant (2nd)] upon NK-cell co-culture. Variability is defined as $v = log2(max(x+1)/min(x+1))$, in which x is a vector of normalized counts across samples. A rule-based decision tree was designed to discriminate the four categories depicted in (**A**). **C,** The percentage of the cell clones in each group on day 14 is depicted for cell lines A, B, C, and D. Shown are the mean values of $n = 2$–3 independent experiments, in which each individual data point represents the mean value ($n = 3$ wells, sequenced in duplicates) of one experiment. **D,** The heatmap shows the normalized abundance of barcodes (norm. BC abundance) of cell line A from one representative experiment ($n = 2$–4 cell lines, four independent experiments). Each subcolumn ($n = 3$) in the figure represents a sample (well), and each row represents a barcode. The barcodes were divided into the four predefined groups according to the criteria defined in (**B**). The Shannon diversity index (shown above the heatmap) serves as measure of barcode diversity and drops significantly after 14 days of NK-cell co-culture. The histogram on the left shows the average abundance of the barcoded cell clone in the B-ALL-only samples on day 4. **E,** The bubble plot depicts the normalized abundance of secondary resistant (2nd) clones in B-ALL samples (day 4) compared with B-ALL + NK samples (day 14). The *x*-axis shows the three individual wells of each condition, whereas each row on the *y*-axis shows an individual tumor cell clone. The size and color of the bubbles indicate the normalized barcode abundance. Shown is the same cell line and experiment as in (**D**). **F,** Comparing two independent experiments in cell line A as shown in (**D** and **E**), the Euler diagrams highlight a high overlap of eliminated, primary resistant (1st), and static cell clones. In contrast, only two secondary resistant (2nd) clones were shared between both independent experiments. (Panel **A** created with BioRender.com. Kovar, H. (2023) BioRender.com/j11m245)

co-cultured with freshly prepared NK cells. As previously observed, B-ALL cells co-cultured with WT NK cells showed an initial susceptibility during the first 2 weeks and developed resistance to NK cells thereafter (**Fig. 4A** and **C**). Co-culture with *Prf1*$^{-/-}$ NK cells only led to a minor growth impairment of the tumor cells (**Fig. 4A**). The presence of *Ifng*$^{-/-}$ NK cells diminished the number of B-ALL cells in the beginning of the co-culture, but the tumor cells became resistant sooner than B-ALL cells co-cultured with WT NK cells (**Fig. 4C**). Five days after B-ALL cells outcompeted NK cells, we measured their resistance to NK cells. A cytotoxicity assay using WT

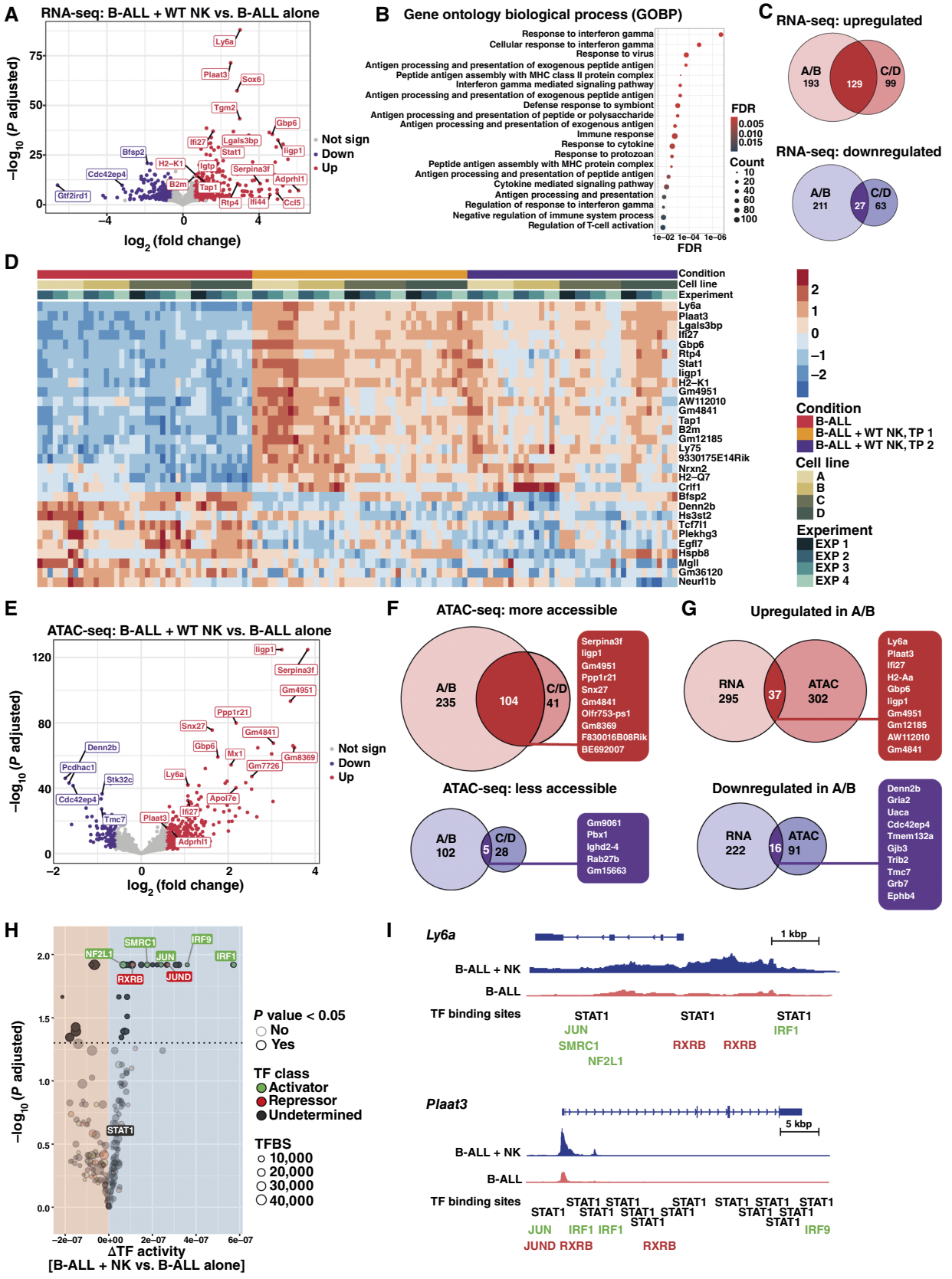

NK cells was performed and showed that in both experiments, B-ALL cells that had been co-cultured with WT NK cells showed the highest NK-cell resistance. *Prf1*$^{-/-}$ and *Ifng*$^{-/-}$ NK cell–co-cultured B-ALL cells were more resistant compared with B-ALL cells cultured alone; however, the resistance was lower than in WT NK co-cultured B-ALL cells (**Fig. 4B** and **D**).

To study the clonal behavior of the tumor cells, the B-ALL cells were analyzed for their barcode diversity on days 4 and 14/17. In line with our previous experiments, the barcode diversity of the B-ALL + WT NK-cell condition dropped significantly in both experiments by approximately 58%. The Shannon diversity of B-ALL cells was decreased by 20% and 40% after co-culture with *Prf1*$^{-/-}$ or *Ifng*$^{-/-}$ NK cells, respectively (**Fig. 4E** and **G**). We observed a strong overlap of eliminated tumor cell clones in all treatment groups, suggesting that these cell clones were *a priori* susceptible to NK cells. In line with fewer eliminated cell clones, we detected more static B-ALL clones upon co-culture with *Prf1*$^{-/-}$ or *Ifng*$^{-/-}$ NK cells (B-ALL + *Prf1*$^{-/-}$ NK cells $n = 420$ vs. B-ALL + WT NK cells $n = 190$; B-ALL + *Ifng*$^{-/-}$ NK cells $n = 281$ vs. B-ALL + WT NK cells $n = 102$). The number of primary and secondary resistant tumor cell clones was similar after co-culture with WT and *Ifng*$^{-/-}$ NK cells (**Fig. 4H**; Supplementary Fig. S8A). In contrast, the presence of *Prf1*$^{-/-}$ NK cells led to a drastically lower number of primary and secondary resistant tumor cell clones (primary resistant: B-ALL + *Prf1*$^{-/-}$ NK cells $n = 96$ vs. B-ALL + WT NK cells $n = 245$; secondary resistant: B-ALL + *Prf1*$^{-/-}$ NK cells $n = 15$ vs. B-ALL + WT NK cells $n = 56$; **Fig. 4F**; Supplementary Fig. S8B). This suggested that the strong immunologic pressure of NK cells leading to the emergence of primary or secondary resistance was driven by cytotoxicity rather than IFNγ production.

To define the molecular changes driving resistance to NK cells, we compared the transcriptomic profiles of B-ALL cells after co-culture with WT and *Prf1*$^{-/-}$ (day 14, **Fig. 4I** and **J**; Supplementary Fig. S9A and S9B) or *Ifng*$^{-/-}$ NK cells (day 17, **Fig. 4K** and **L**; Supplementary Fig. S9C and S9D and day 32, Supplementary Fig. S9E–S9H). B-ALL cells after culture with WT or *Prf1*$^{-/-}$ NK cells showed an overlap of 28 upregulated and 18 downregulated DEGs, including *Ly6a* and *Plaat3* (**Fig. 4I** and **J**; Supplementary Fig. S9A and S9B, respectively). Intriguingly, B-ALL cells only showed marginal changes in their transcriptome when cultured with *Ifng*$^{-/-}$ NK cells (B-ALL + *Ifng*$^{-/-}$ NK cells vs. B-ALL alone: $n = 3$ DEGs; B-ALL + WT NK cells vs. B-ALL alone: $n = 412$ DEGs, **Fig. 4K** and **L;** Supplementary Fig. S9C–S9H). This highlights the pivotal role of IFNγ and argues against a major contribution of other NK cell–derived cytokines in driving the observed transcriptional changes in NK cell–resistant B-ALL cells. Accordingly, only B-ALL cells cultured in the presence of IFNγ-producing WT NK cells induced the expression of ligands for NK-cell receptors, such as components of the classical and non-classical MHC-I machinery (Supplementary Fig. S9I and S9J).

In conclusion, while NK-cell cytotoxicity was pivotal for the induction of primary and secondary resistance in tumor cells, IFNγ production induced an NK cell–resistant phenotype on the transcriptomic level. The combination of NK-cell cytotoxicity and IFNγ production was needed for selecting and sculpting resistant tumor cells and ultimately for tumor immunoediting.

The role of PLAAT3 and Ly6A/LY6E in tumor evasion of NK cell–mediated killing

NK-cell resistance in B-ALL cells was associated with altered expression of well-known and genes not previously, to our knowledge, involved in cancer immunoediting. We demonstrated in multiple experiments that *Plaat3* and *Ly6a* belonged to the most significantly upregulated genes in NK cell–resistant B-ALL cell lines. Therefore, we followed up on these genes and studied their role in immune evasion. We performed a similar co-culture experiment as before and analyzed the B-ALL cells on day 14 by mass spectrometry to confirm the upregulation of PLAAT3 and Ly6A on the protein level. Indeed, PLAAT3 and Ly6A were increased after WT or *Prf1*$^{-/-}$ NK-cell co-culture and even more upon recombinant IFNγ treatment (**Fig. 5A**; Supplementary Fig. S10A). We confirmed that the IFNγ-dependent upregulation of Ly6A in B-ALL cells in NK-cell co-cultures was stable, as it persisted several days after the NK cells were gone from the co-culture (**Fig. 5B**).

To study the role of PLAAT3 in more detail, we generated *Plaat3* KO B-ALL clones and verified the lack of *Plaat3* mRNA by qPCR (Supplementary Fig. S10B). *Plaat3* KO cells did not show any difference in proliferation and viability, induction of IFNγ production by NK cells, and expression of NK cell–receptor ligands (Supplementary Fig. S10C–S10F). Moreover, loss of *Plaat3* did not affect direct NK cell–mediated killing of mouse B-ALL cells (Supplementary Fig. S10G). To test the relevance of the human orthologue *PLAAT3* in leukemia, we analyzed *PLAAT3* expression of patients with ALL and observed an insignificant trend of worse overall survival in patients with increased *PLAAT3* expression (Supplementary Fig. S10H). These results suggested that although PLAAT3 expression was upregulated

Figure 3.

Integrative analysis of RNA and ATAC sequencing shows well-known and novel genes deregulated in NK cell–resistant B-ALL cells. The (**A–D** and **G**) transcriptome and (**E–I**) chromatin accessibility analysis of B-ALL cells co-cultured with NK cells for 4 [time point 1 (TP1)] or 14 (TP2) days were analyzed and compared with the B-ALL-alone cells on TP1 ($n = 3$–4 independent experiments). **A,** The volcano plot shows the significantly upregulated or downregulated genes in B-ALL cell lines A and B after co-culture with NK cells for 14 days ($n = 3$ experiments). Statistics were calculated using the Wald test. **B,** The dot plot illustrates the enrichment analysis using the hyperR tool (28) for the Gene Ontology Biological Process (GOBP) terms associated with NK-cell co-cultured B-ALL cells shown in **A**. *X*-axis and dot color depict the false discovery rate (FDR) and *y*-axis the corresponding biological processes. Dot size illustrates the number of genes associated with the biological processes. **C,** The Euler diagrams display upregulated or downregulated genes in cell lines A/B and/or C/D after 14 days of NK-cell co-culture. **D,** The heatmap shows the expression of selected overlapping genes (top 20 upregulated, top 10 downregulated; ranked by *P* value) identified in **C** ($n = 3$–4 experiments, four B-ALL cell lines). The row-scaled normalized counts represent the $\log_2$(fold change). **E,** The volcano plot shows differentially accessible regions in B-ALL cells A/B after co-culture with NK cells for 14 days ($n = 3$ experiments). Statistics were calculated using the Wald test. **F,** The Euler diagrams highlight genes in which promoters (transcription start site ± 3 kb) had higher or lower chromatin accessibility in cell lines A/B and/or C/D after 14 days of NK-cell co-culture in $n = 3$–4 experiments. Gene promoters with the highest $\log_2$(fold change) are highlighted. **G,** Integration of RNA and ATAC sequencing data shows that 37 genes are upregulated and 16 downregulated in cell lines A/B; the top 10 upregulated or downregulated genes are highlighted on the right. **H,** Analysis of differential transcription factors activity using diffTF (37) highlighted activator (green) and repressor (red) TFs that were differentially expressed in B-ALL cell lines A/B after NK-cell co-culture. **I,** Integrative Genomics Viewer (IGV) genome browser tracks display representative ATAC sequencing signal densities ($n = 3$ experiments) at the *Ly6a* and *Plaat3* loci in B-ALL cells with or without NK-cell co-culture. Shown are the gene bodies including a 3-kb upstream promoter region, as well as binding sites of TFs identified in (**H**). Database HOCOMOCO (v10; ref. 38) was used, and depicted are counts per million (CPM) with a range of (0–1.37).

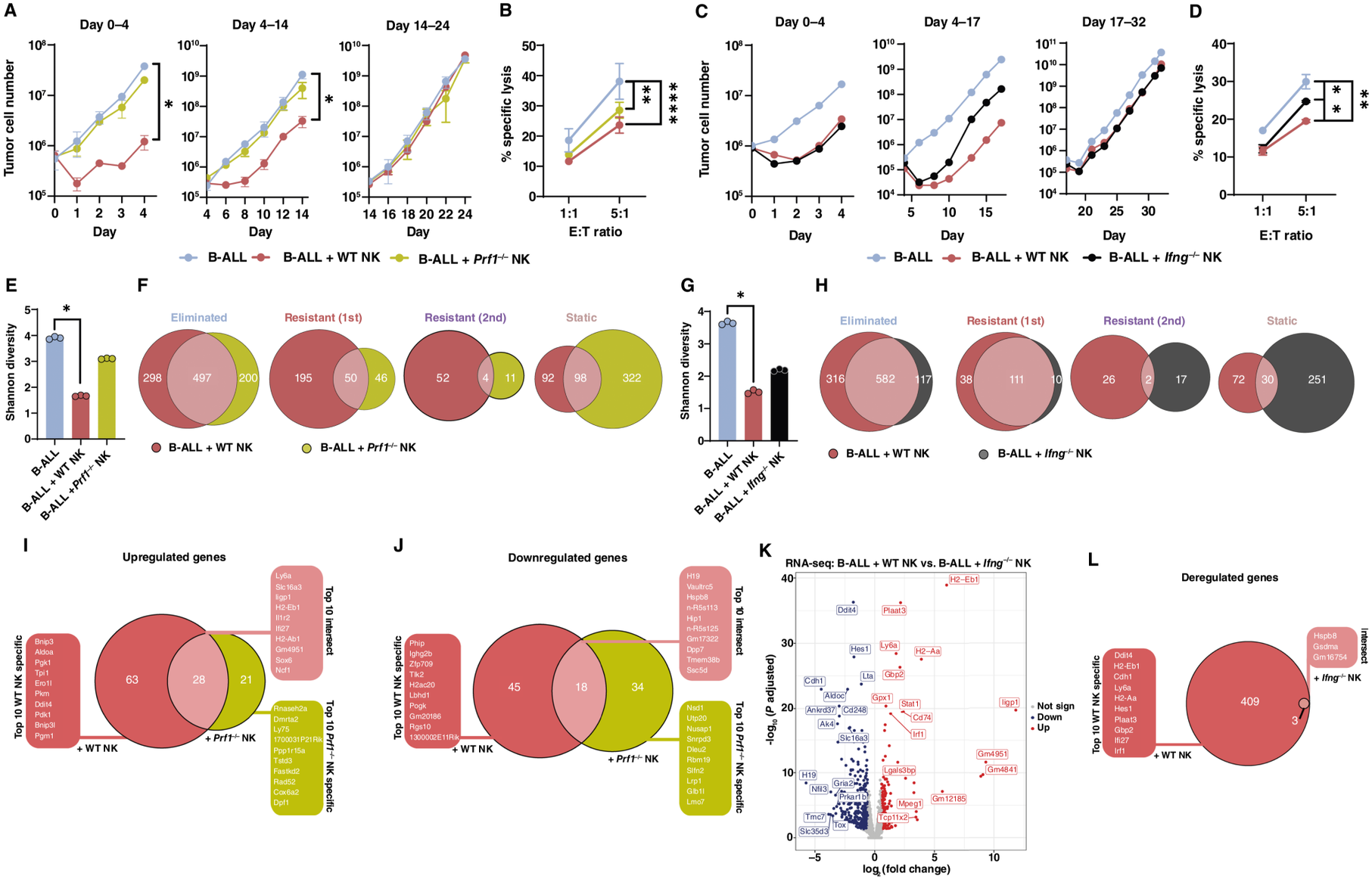

Figure 4.

The combination of NK-cell cytotoxicity and IFNγ production drives tumor immunoediting. **A** and **C,** Barcoded B-ALL cell lines ($n = 2$ cell lines A/D) were cultivated in three individual wells either in the absence or presence of purified and IL2-activated WT, (**A**) *Prf1*$^{-/-}$, or (**C**) *Ifng*$^{-/-}$ NK cells. Absolute numbers of B-ALL cells were determined by flow cytometry. On days 0, 4, and 14/17 B-ALL cells were FACS sorted and replated, and fresh NK cells were replenished. **A,** Shown are means ± SD of $n = 2$ cell lines. The significance was calculated using the Kruskal–Wallis test and Dunn's multiple comparisons testing. **C,** Shown is one cell line ($n = 2$) of two independent experiments. **B** and **D,** On the last day of the NK-cell co-culture experiment, a 4-hour NK cytotoxicity assay with WT NK cells was performed using B-ALL cells that had been cultured for 4 weeks in the presence or absence of NK cells. Statistics were calculated for the highest E:T ratio with one-way ANOVA with Tukey's multiple comparisons test. **B,** Shown are means ± SD of technical triplicates. **D,** Shown are means ± SD of technical duplicates. **E** and **G,** The Shannon diversity of leukemic clones dropped significantly ($P = 0.02$) upon co-culture with WT NK cells and to a lesser degree with (**E**) *Prf1*$^{-/-}$ or (**G**) *Ifng*$^{-/-}$ NK cells. Shown is the mean, and dots depict each replicate. Statistics were calculated using the Kruskal–Wallis and Dunn's multiple comparisons testing. **F** and **H,** The barcodes within each sample were classified according to the decision tree in **Fig. 2B**. The barcodes that were attributed to the four predefined groups were compared between the treatment groups with Euler diagrams for each group [eliminated, resistant (1st), resistant (2nd), and static]. **I** and **J,** The Euler diagrams display the number of upregulated and downregulated genes in cell lines A/D after 14 days of co-culture with WT or *Prf1*$^{-/-}$ NK cells. Top 10 upregulated or downregulated genes in the intersection or specific for WT or *Prf1*$^{-/-}$ NK-cell co-culture are depicted in the corresponding lists. **K,** The volcano plot depicts DEGs in B-ALL + WT NK versus B-ALL + *Ifng*$^{-/-}$ NK conditions on day 17 of cell line A. **L,** The Euler diagram depicts DEGs when comparing B-ALL + WT or B-ALL + *Ifng*$^{-/-}$ NK conditions with B-ALL alone. Top 10 WT NK cell–specific genes and the three overlapping genes are depicted in the corresponding lists. Shown is (**A**, **B**, **I**, and **J**) one experiment including $n = 2$ cell lines A/D or (**C–H**, **K**, and **L**) one experiment from cell line A. Data in **A–D** are representative for two independent experiments and $n = 2$ cell lines. *, $P < 0.05$; **, $P < 0.01$; ****, $P < 0.0001$.

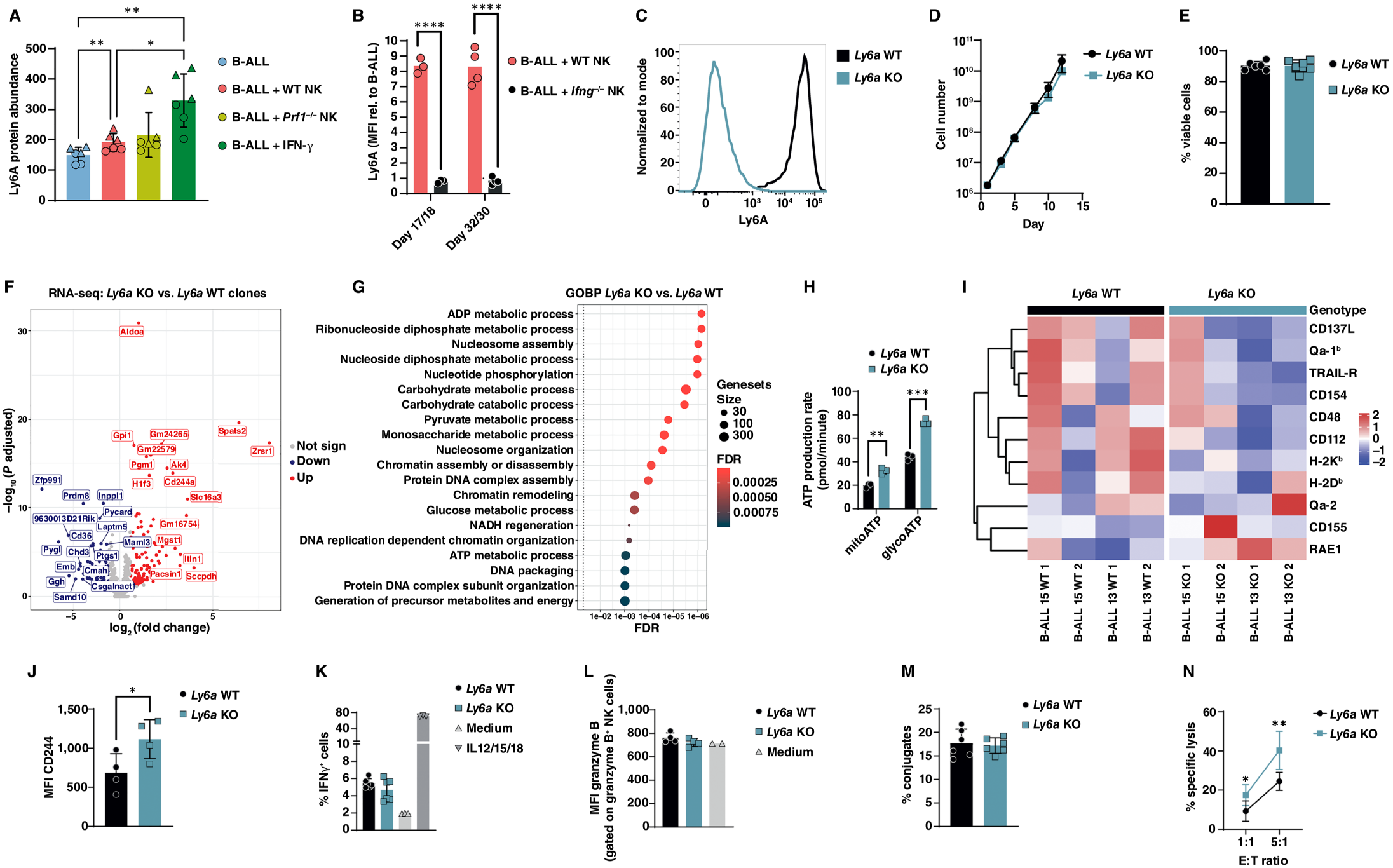

Figure 5.

The role of mouse Ly6A in the evasion of leukemic cells from NK cell–mediated surveillance. **A,** The bar graph shows the protein abundance of Ly6A on day 14 of the same co-culture experiments as described in **Fig. 4A** with continuous IFNγ treatment as additional condition. Two B-ALL cell lines (A in circles/D in triangles) were analyzed by mass spectrometry in triplicates. Bars and error bars represent means of arbitrary units (AU) relative to the whole protein abundance ± SD; the significance was calculated by one-way ANOVA with Tukey's multiple comparisons test. **B,** Ly6A surface expression was measured on B-ALL cells co-cultured with WT or *Ifng*$^{-/-}$ NK cells for 17/18 or 32/30 days. Bars represent means ($n = 3$–4 for cell line D from two independent experiments); statistics were calculated using an unpaired *t* test. **C,** *Ly6a* KO clones were generated by CRISPR/Cas9 genome editing in parental B-ALL cell lines. The gene modification was verified by measuring Ly6A surface expression by flow cytometry. Histogram shows the Ly6A expression in one representative *Ly6a* WT and KO clone ($n = 6$). **D,** Growth curve of *Ly6a* WT and KO B-ALL clones in absolute cell numbers was measured for 13 days. Shown are means ± SD of $n = 2$ clones per genotype, measured in technical duplicates. **E,** Cell viability of *Ly6a* WT and KO B-ALL clones. Shown are means ± SD of $n = 2$ clones per genotype of $n = 3$ independent experiments. **F,** The volcano plot shows DEGs ($n = 342$) in *Ly6a* KO versus *Ly6a* WT clones ($n = 2$ clones per genotype, sequenced in technical triplicates) under normal culturing conditions. Differentially upregulated or downregulated genes are depicted in red and blue, respectively. Statistics were calculated using the Wald test. **G,** The dot plot illustrates the Gene Ontology Biological Process (GOBP) terms associated with *Ly6a* deficiency in B-ALL cells shown in (**F**). *X*-axis and dot color depict the false discovery rate (FDR) and *y*-axis the corresponding biological processes. Dot size illustrates the number of genes associated with the biological processes. **H,** An ATP rate assay was performed in *Ly6a* WT and KO cells. Bar graph depicts means ± SD of mitochondrial and glycolytic ATP production; the significance was calculated using an unpaired *t* test. **I,** *Ly6a* WT and KO B-ALL cell lines ($n = 4$ per genotype) were characterized by their surface expression of NK cell–receptor ligands by flow cytometry. Columns represent different tumor cell clones ordered according to genotype and cell line. Data were scaled and clustered by row to highlight variations in marker expression across different samples. Red indicates higher and blue lower expression levels of surface ligands. **J,** The expression of CD244 on the surface of *Ly6a* WT and KO clones was determined by flow cytometry. The bars and error bars represent the mean ± SD of the MFIs of $n = 2$ clones per genotype and two independent experiments. Statistics were calculated using an unpaired *t* test. **K,** IFNγ-producing mNK cells upon co-culture with *Ly6a* WT and KO B-ALL cell lines for 4 hours ($n = 2$ clones per genotype and technical triplicates) were measured by flow cytometry. As a positive control, mNK cells were activated with IL12/IL15/IL18. **L,** Granzyme B production in freshly isolated NK cells was determined after co-culture with *Ly6a* WT and KO clones for 4 hours. Shown are means ± SD of $n = 2$ clones per genotype and two independent experiments. **M,** *Ly6a* WT and KO B-ALL cell clones were co-incubated with WT NK cells for 10 minutes before the flow cytometric-based assessment of tumor–NK-cell conjugate formation ($n = 6$ clones per genotype). Shown is one representative experiment ($n = 3$ experiments with $n = 2$–6 clones per genotype). **N,** A 4-hour NK cytotoxicity assay was performed using *Ly6a* WT and KO B-ALL clones. Shown are means ± SD of $n = 2$ clones per genotype and three independent experiments; statistics were calculated using an unpaired *t* test. *, $P < 0.05$; **, $P < 0.01$; ****, $P < 0.0001$.

by IFNγ and correlated with resistance to NK cells, it does not seem to be a functional driver of tumor evasion.

Likewise, we deleted *Ly6a* in B-ALL cells and verified the lack of Ly6A surface protein expression by flow cytometry (**Fig. 5C**). Ly6A deficiency had no impact on B-ALL cell proliferation or survival (**Fig. 5D** and **E**). To investigate the impact of Ly6A on the transcriptomic level, we performed RNA sequencing of *Ly6a* WT and KO B-ALL cells and found 127 upregulated and 80 downregulated genes mainly related to metabolic processes (**Fig. 5F** and **G**). In line with these results, we observed an increase in mitochondrial and glycolytic ATP production in *Ly6a* KO cells (**Fig. 5H**). Increased tumor metabolism may induce the expression of stress ligands and consequently lead to better activation of NK cells (47). Although most classical NK cell–receptor ligands showed unaltered expression, we observed a slightly higher expression of RAE1 ($P = 0.08$, unpaired *t* test) and lower expression of CD112 ($P = 0.04$) in B-ALL cells lacking Ly6A (**Fig. 5I**). Further, CD244 was upregulated in *Ly6a* KO cells on the RNA and protein levels (**Fig. 5F** and **J**). CD244 is a marker known to be present on NK cells (48) but only basally expressed in mouse marginal-zone B cells (49) with a reported function in B-cell differentiation and autoimmunity (50). We tested the functional consequences of *Ly6a* deficiency for the interaction of B-ALL and NK cells. We detected unaltered IFNγ (**Fig. 5K**) and granzyme B production (**Fig. 5L**) upon co-culture with B-ALL cells and similar numbers of tumor–NK-cell conjugates (**Fig. 5M**) irrespective of the presence or absence of *Ly6a*. However, *Ly6a* KO B-ALL cells were more susceptible to NK cell–mediated killing compared with WT cells in cytotoxicity assays (**Fig. 5N**). These results show that Ly6A plays an important role in NK cell–mediated immune evasion of mouse B-ALL cells.

LY6E has been described as a close relative of Ly6A in the human system (51, 52). High *LY6E* expression correlated significantly with poor survival in patients with ALL (**Fig. 6A**). To further study the human relevance of our findings, we generated *LY6E*-deficient BCR/ABL1$^+$ K562 cells and verified the lack of LY6E protein expression by immunoblotting. In line with previous reports (53), we detected an IFNβ-dependent upregulation of LY6E in K562 cells (**Fig. 6B**). Transcriptomic analysis of *LY6E* WT and KO K562 cells showed a total of 829 deregulated genes (454 up and 375 down, **Fig. 6C**), which were mainly associated to cell death, cell cycle, and intracellular transport (**Fig. 6D**). However, we did not observe any significant differences in cell proliferation or viability between *LY6E* WT and KO clones (**Fig. 6E** and **F**). When analyzing the interaction of NK cells with *LY6E* WT and KO clones, we found no difference in NK-cell IFNγ and TNFα production (Supplementary Fig. S11) but a tendency for an increased NK-cell susceptibility of the *LY6E* KO clones (**Fig. 6G**). We did detect that *LY6E* KO clones formed significantly more tumor–NK conjugates compared with *LY6E* WT cells (**Fig. 6H**).

In summary, our functional analysis of PLAAT3 and Ly6A showed that their expression is upregulated in tumor cells co-cultured with NK cells in an IFNγ-dependent manner. Although PLAAT3 was persistently upregulated in our multiomics analysis, it proved to have no effect on NK-cell resistance. In contrast, Ly6A and LY6E were identified as drivers of tumor evasion by impairing the interaction of NK and tumor cells.

Discussion

NK cells represent a potent arm of the immune system, tasked with eliminating malignant cells. Nonetheless, they can fail to eradicate all cancer cells, which spares some that have successfully evaded the immune surveillance. The present study aimed to elucidate the mechanisms employed by tumor cells to escape NK cells. Our study is based on heterogeneous, non-edited, and immune–naïve mouse BCR/ABL^{p185+} B-ALL tumor cell lines, which were co-cultured for several weeks with mNK cells. This model enabled us to explore the primary interplay between tumor cells and the immune system. Furthermore, the B-ALL tumor cells were DNA barcoded, a technique that allows for the quantification of tumor cell clonal dynamics and a better understanding of NK-cell effector functions. To the best of our knowledge, this particular aspect has not been demonstrated in previous studies. The determination of tumor cell fate during the co-culture revealed that most tumor cell clones possessed inherent sensitivity or resistance to NK cells. DNA barcoding has already been used by others to quantify tumor cell susceptibility toward immune cells and drug- or antibody-based immunotherapies [54–57]. Similar to our research, these studies observed that most tumor cells are predestined for being sensitive or resistant to treatment. Our study highlighted tumor cell clones beyond those two fundamental fates of life and death, which acquired secondary resistance in the presence of NK cells. Secondary resistance, defined as the occurrence of resistance in one of three replicate wells after 2 weeks of co-culture, was only observed in a small subset of tumor cell clones. Similarly, using DNA barcoding to investigate the clonal evolution of drug-treated lung cancer cells, Acar and colleagues [54] recently described the emergence of "*de novo* resistant lineages" in one replicate only. We found that secondary resistant tumor cells were highly distinctive for each independently performed experiment, suggesting that a stochastic event causes the resistance. However, because of the necessity of expanding the barcoded cell lines before the experiments (to ensure reproducible representation of all barcodes in every well), we cannot formally exclude the possibility of preexisting heterogeneity within a cell clone. Furthermore, the barcode sequence of the LG2.1 library was found to be located approximately 900 bps upstream of the polyA tail and could thus not be detected using single-cell RNA sequencing. It would certainly be interesting to delve deeper into secondary resistance mechanisms and to compare the transcriptomic profiles of primary and secondary resistant tumor cell clones in the future (58, 59).

In summary, the DNA barcode analysis demonstrated that NK cells can shape tumor cells and contribute to immunoediting of tumor cell clones. To dissect the two main functions of NK cells, namely, killing tumor cells and producing IFNγ, we analyzed the clonal evolution of B-ALL cells co-cultured with *Prf1*$^{-/-}$ and *Ifng*$^{-/-}$ NK cells, respectively. It is widely acknowledged that IFNγ is a major player in cancer immunoediting [60]. In our experiments, tumor cells responded to the NK-cell co-culture with an upregulation of many IFNγ inducible genes, such as MHC-I molecules, thereby inhibiting NK cells and inducing resistance. Interestingly, and against our expectations, we observed a similar number of primary and secondary resistant B-ALL cell clones upon co-culture with WT or *Ifng*$^{-/-}$ NK cells. On the contrary, co-culture with *Prf1*$^{-/-}$ NK cells led to fewer primary and secondary resistant B-ALL cell clones. This clearly suggested that the selection of *a priori* resistant tumor cell clones and the acquisition of secondary resistance was mainly because of NK cell–mediated killing rather than IFNγ production. However, the transcriptomic changes observed in long-term co-cultured B-ALL cells were only partially affected by loss of NK cell–killing capacity but completely absent in B-ALL cells

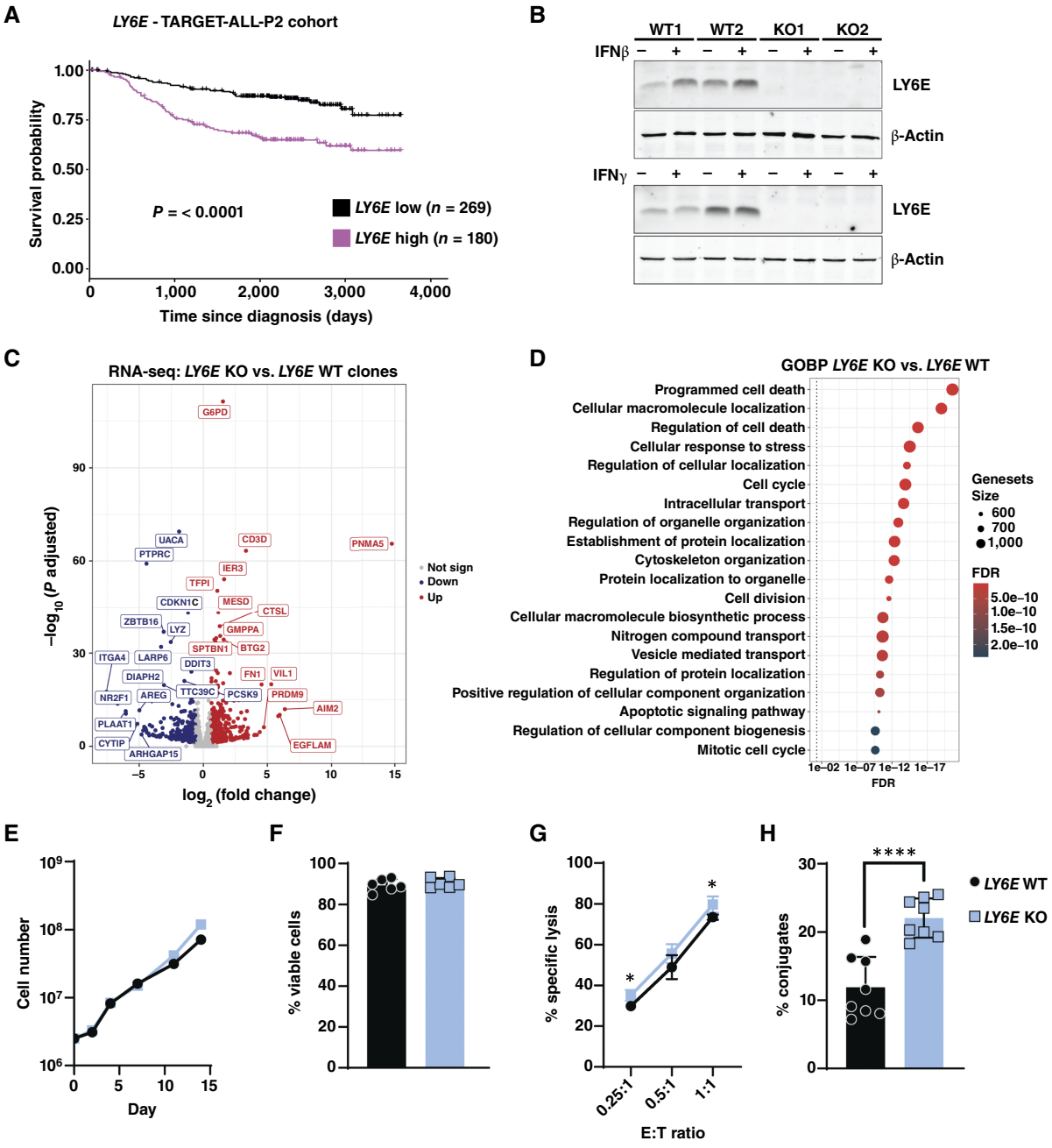

Figure 6.

The role of human LY6E in the evasion of leukemic cells from NK cell–mediated surveillance. **A,** The Kaplan–Meier plot depicts survival probabilities of the TARGET-ALL-P2 patient cohort divided into *LY6E* high- and low-expressing groups (cutoff percentile = 60%). The graph was generated by the online web tool cSurvival(ubc.ca). **B,** *LY6E* WT and KO K562 clones were analyzed for their expression of LY6E in the absence or presence of IFNβ (top) or IFNγ (bottom) by Western blotting. β-actin served as a loading control. **C,** The volcano plot shows DEGs ($n = 829$) in *LY6E* KO versus *LY6E* WT K562 clones under normal culturing conditions ($n = 2$ clones per genotype, sequenced in technical triplicates). Differentially upregulated or downregulated genes are depicted in red and blue, respectively. Statistics were calculated using the Wald test. **D,** The dot plot illustrates the Gene Ontology Biological Process (GOBP) terms associated with *LY6E* deficiency in K562 cells shown in **C**. *X*-axis and dot color depict the false discovery rate (FDR) and *y*-axis the corresponding biological processes. Dot size illustrates the number of genes associated with the biological processes. **E,** Growth curve of *LY6E* WT and KO K562 clones in absolute cell numbers was measured for 14 days. Shown is one clone per genotype, representative of two clones. **F,** Cell viability of *LY6E* WT and KO K562 clones. Shown are means ± SD of $n = 2$ cell lines per genotype and three independent experiments. **G,** A 1-hour NK cytotoxicity assay was performed using *LY6E* WT and KO K562 clones. Shown are means ± SD of technical duplicates of $n = 2$ clones per genotype and two independent experiments using NK cells isolated from two different donors. Statistics were calculated using an unpaired *t* test. **H,** *LY6E* WT and KO clones were co-incubated with NK cells, and the tumor–NK-cell conjugate formation was assessed by flow cytometry. Bars and error bars represent means ± SD of $n = 2$ clones per genotype and four independent experiments using NK cells isolated from four different donors. Statistics were calculated using an unpaired *t* test.*, $P < 0.05$; ****, $P < 0.0001$.

cultured with *Ifng*$^{-/-}$ NK cells. This data argues against a major contribution of other NK cell–derived cytokines such as TNFα on the tumor immunoediting process. We thus concluded that although IFNγ plays only a minor role in tumor cell selection, it enhances NK-cell resistance of the remaining tumor cells by upregulating IFNγ-dependent genes, such as genes involved in MHC-I presentation and *Ly6a*.

Among others, previously described mechanisms by which tumors evade NK cells include the upregulation of proteins involved in antigen presentation and MHC-I and MHC-II molecules (61, 62), the loss or shedding of NKG2D ligands such as MHC class I chain-related molecule A and B (MICA/B; ref. 63), and the secretion of TGFβ and IL10 (64). We here describe *Ly6a* overexpression as a driver of tumor evasion by impairing NK cell–mediated killing. Ly6A, also called stem cell antigen-1 (Sca-1), is an 18-kDa mouse glycosylphosphatidylinositol-anchored cell surface protein. It plays an important role in hematopoietic progenitor/stem cell lineage fate, brain–blood barrier transport, and cancer stem cell (CSC) biology (65–68). Ly6A has been shown to be upregulated in CSCs and many tumor entities and is induced by Wnt/β-catenin signaling and TGFβ deregulation. This promotes cell adhesion and migration *in vitro*, increased tumorigenicity, and resistance to chemotherapy *in vivo* (68–71). The human LY6 gene family comprises several members, but the direct orthologue of mouse *Ly6a* has been under debate for a long time. *LY6A/LY6S* was just recently discovered, probably because of its genomic localization on the opposite strand of and highly overlapping with *LY6S-AS1/C8orf31/LINC02904* (51, 72). The expression of *LY6A/LY6S* seems to be restricted to pituitary tumors (72) and a subset of nonclassical lymphoid cells of the spleen (51), and it could not be detected in hematopoietic cell lines (72) or leukemia samples isolated from patients. Besides *LY6A/LY6S*, other *LY6* family members have been suggested as close homologues of the murine *Ly6a* gene, such as *LY6D*, *LY6E*, *LY6H*, and *LY6K*, which were implicated as biomarkers for poor cancer prognosis and are frequently amplified in human cancer (52). Al Hossiny and colleagues showed that human LY6E promotes breast cancer *in vivo* and drives drug sensitivity and epithelial-to-mesenchymal transition. Moreover, they observed that LY6E is required for TGFβ signaling and facilitates immune evasion by upregulating PD-L1 on cancer cells, by recruiting regulatory T cells and dampening NK-cell activation (73). Consistent with this, our survival analysis of a pediatric ALL patient cohort confirmed the cancer driving feature of LY6E also in leukemia. Our data show that NK cells are less likely to form conjugates with human leukemic cells in the presence of LY6E, which ultimately resulted in a minor increase in susceptibility to NK cells. In summary, this substantiates the reported oncogenic and immune suppressive properties of human LY6E and murine Ly6A, but the exact mechanism remains unknown. Although Ly6A has not been directly associated with cell metabolism, our data indicated that *Ly6a* KO B-ALL cells produced more ATP through glycolysis and oxidative phosphorylation. Increased metabolism is generally associated with immune suppression and NK-cell inhibition (74), which is contradictory to our observed phenotype. However, it was also shown that increased glycolysis can enhance the expression of NK cell–activating NKG2D ligands (47). We only observed a slight and insignificant increase of RAE1 on *Ly6a* KO B-ALL cells, besides differences in CD112 and CD244 expression. It has been suggested that Ly6A regulates the clustering of receptors or ligands within lipid rafts on the cell membrane (75). We thus hypothesize that potential differences in local concentrations of NK cell–receptor ligands may contribute to the lower susceptibility of Ly6A–expressing B-ALL cells to NK cell–mediated killing, but this notion needs further evaluation.

Considering the association of *Ly6a* with cancer stemness, our findings align with the concept that immunoedited and thus more aggressive tumor cells may harbor CSC features. CSCs are considered responsible for metastasis and therapy resistance, as they are characterized by deregulated differentiation, self-renewal, drug resistance, and evasion of immunosurveillance, among others. Unlike other immune cells, NK cells are believed to show direct cytotoxicity against CSCs (76). By contrast, as CSCs frequently upregulate classical and nonclassical MHC-I molecules while losing NK cell–activating ligands, it is still a matter of debate if and how NK cells are able to detect and kill CSCs (76, 77).

In conclusion, our work sheds light on the intricate interplay between NK cells and leukemic cells during initial encounters. This study shows that leukemic cells are actively shaped by NK cells and unravels what we believe to be novel cancer evasion strategies by identifying potential driver genes in mice (*Ly6a*) and humans (*LY6E*). Further research, especially *in vivo* and with single-cell resolution, is required to delve deeper into primary and secondary resistance mechanisms and the general role of Ly6A and LY6E in NK cell–mediated tumor surveillance. These findings ultimately deepen our understanding of the initial interaction between tumor and NK cells and of cancer immune evasion in general.

Authors' Disclosures

P. Repiscak reports other support from Boehringer Ingelheim outside the submitted work. A.R. Poetsch reports grants from German Cancer Aid during the conduct of the study. No disclosures were reported by the other authors.

Authors' Contributions

M.C. Buri: Formal analysis, funding acquisition, investigation, visualization, methodology, writing–original draft, project administration, writing–review and editing. **M.R. Shoeb:** Formal analysis, visualization, writing–review and editing. **A. Bykov:** Formal analysis, visualization, writing–review and editing. **P. Repiscak:** Formal analysis, visualization, writing–review and editing. **H. Baik:** Formal analysis, investigation, writing–review and editing. **A. Dupanovic:** Formal analysis, investigation, visualization, writing–review and editing. **F.O. David:** Formal analysis, investigation, writing–review and editing. **B. Kovacic:** Formal analysis, investigation, visualization, methodology, writing–review and editing. **F. Hall-Glenn:** Investigation, writing–review and editing. **S. Dopa:** Investigation, writing–review and editing. **J. Urbanus:** Resources, methodology, writing–review and editing. **L. Sippl:** Investigation, writing–review and editing. **S. Stofner:** Investigation, writing–review and editing. **D. Emminger:** Investigation, writing–review and editing. **J. Cosgrove:** Resources, methodology, writing–review and editing. **D. Schinnerl:** Formal analysis, writing–review and editing. **A.R. Poetsch:** Formal analysis, writing–review and editing. **M. Lehner:** Resources, methodology, writing–review and editing. **X. Koenig:** Visualization, writing–review and editing. **L. Perié:** Resources, methodology, writing–review and editing. **T.N. Schumacher:** Resources, methodology, writing–review and editing. **D. Gotthardt:** Formal analysis, investigation, methodology, writing–review and editing. **F. Halbritter:** Formal analysis, supervision, funding acquisition, writing–review and editing. **E.M. Putz:** Conceptualization, resources, formal analysis, supervision, funding acquisition, validation, investigation, visualization, methodology, writing–original draft, project administration, writing–review and editing.

Acknowledgments

We thank Veronika Sexl (University of Veterinary Medicine, Vienna, Austria) for providing the BCR/ABL^{p185} construct, Thomas Kolbe (University of Veterinary Medicine, Vienna, Austria) for providing the *B2m*$^{-/-}$ mice, and Sabine Strehl and Klaus Fortschegger (CCRI, Austria) for discussions and sharing information. We are grateful to Marcus Toetzl for assistance with ATAC-seq library preparation and Melanie Hofmann and Gernot Schabbauer for support with the Seahorse experiments. We thank the CCRI FACS and Bioinformatics Core Units for assistance with cell sorting

and bioinformatics/statistics, respectively, the Core Facility Laboratory Animal Breeding and Husbandry of the Medical University of Vienna (MUW, Austria) for taking care of our mice, and the Biomedical Sequencing Facility and the Proteomics Facility of the CeMM Research Center for Molecular Medicine of the Austrian Academy of Sciences for their support on next-generation sequencing and mass spectrometry analysis, respectively. This work was supported by St. Anna Children's Cancer Research Institute (Vienna, Austria), by a DOC fellowship of the Austrian Academy of Sciences awarded to M.C. Buri (#25905), and by grants from the Fellinger Krebsforschung to E.M. Putz and from the Austrian Science Fund (10.55776/P32001, 10.55776/P34832, and 10.55776/WKP132 to E.M. Putz; 10.55776/TAI454 and 10.55776/TAI732 to F. Halbritter; 10.55776/P31563 and 10.55776/I4649 to X. Koenig). F. Halbritter was supported by funding from the Alex's Lemonade Stand Foundation for Childhood Cancer (20-17258), and A.R. Poetsch was supported by the Mildred Scheel Early Career Center Dresden P2, funded by the German Cancer Aid.

Note

Supplementary data for this article are available at Cancer Immunology Research Online (http://cancerimmunolres.aacrjournals.org/).

Received February 22, 2024; revised September 27, 2024; accepted December 4, 2024; published first December 6, 2024.

References

1. Gubin MM, Vesely MD. Cancer immunoediting in the era of immuno-oncology. Clin Cancer Res 2022;28:3917–28.
2. Dunn GP, Bruce AT, Ikeda H, Old LJ, Schreiber RD. Cancer immunoediting: from immunosurveillance to tumor escape. Nat Immunol 2002;3:991–8.
3. Wolf NK, Kissiov DU, Raulet DH. Roles of natural killer cells in immunity to cancer, and applications to immunotherapy. Nat Rev Immunol 2023;23:90–105.
4. Metkar SS, Wang B, Aguilar-Santelises M, Raja SM, Uhlin-Hansen L, Podack E, et al. Cytotoxic cell granule-mediated apoptosis: perforin delivers granzyme B-serglycin complexes into target cells without plasma membrane pore formation. Immunity 2002;16:417–28.
5. Prager I, Watzl C. Mechanisms of natural killer cell-mediated cellular cytotoxicity. J Leukoc Biol 2019;105:1319–29.
6. Wang W, Erbe AK, Hank JA, Morris ZS, Sondel PM. NK cell-mediated antibody-dependent cellular cytotoxicity in cancer immunotherapy. Front Immunol 2015;6:368.
7. Bald T, Krummel MF, Smyth MJ, Barry KC. The NK cell–cancer cycle: advances and new challenges in NK cell–based immunotherapies. Nat Immunol 2020;21:835–47.
8. O'Sullivan T, Saddawi-Konefka R, Vermi W, Koebel CM, Arthur C, White JM, et al. Cancer immunoediting by the innate immune system in the absence of adaptive immunity. J Exp Med 2012;209:1869–82.
9. López-Soto A, Gonzalez S, Smyth MJ, Galluzzi L. Control of metastasis by NK cells. Cancer Cell 2017;32:135–54.
10. Liu E, Marin D, Banerjee P, Macapinlac HA, Thompson P, Basar R, et al. Use of CAR-transduced natural killer cells in CD19-positive lymphoid tumors. N Engl J Med 2020;382:545–53.
11. Bernareggi D, Xie Q, Prager BC, Yun J, Cruz LS, Pham TV, et al. CHMP2A regulates tumor sensitivity to natural killer cell-mediated cytotoxicity. Nat Commun 2022;13:1899.
12. Chiba M, Shimono J, Ishio T, Takei N, Kasahara K, Ogasawara R, et al. Genome-wide CRISPR screens identify CD48 defining susceptibility to NK cytotoxicity in peripheral T-cell lymphomas. Blood 2022;140:1951–63.
13. Pech MF, Fong LE, Villalta JE, Chan LJ, Kharbanda S, O'Brien JJ, et al. Systematic identification of cancer cell vulnerabilities to natural killer cell-mediated immune surveillance. Elife 2019;8:e47362.
14. Sheffer M, Lowry E, Beelen N, Borah M, Amara SNA, Mader CC, et al. Genome-scale screens identify factors regulating tumor cell responses to natural killer cells. Nat Genet 2021;53:1196–206.
15. Carré T, Thiery J, Janji B, Terry S, Gros G, Meurice G, et al. Selection of tumor-resistant variants following sustained natural killer cell-mediated immune stress. Oncol Rep 2021;45:582–94.
16. Dufva O, Gandolfi S, Huuhtanen J, Dashevsky O, Duàn H, Saeed K, et al. Single-cell functional genomics reveals determinants of sensitivity and resistance to natural killer cells in blood cancers. Immunity 2023;56:2816–35.e13.
17. Naik SH, Schumacher TN, Perié L. Cellular barcoding: a technical appraisal. Exp Hematol 2014;42:598–608.
18. Eisele AS, Cosgrove J, Magniez A, Tubeuf E, Tenreira Bento S, Conrad C, et al. Erythropoietin directly remodels the clonal composition of murine hematopoietic multipotent progenitor cells. Elife 2022;11:e66922.
19. Marsolier J, Prompsy P, Durand A, Lyne A-M, Landragin C, Trouchet A, et al. H3K27me3 conditions chemotolerance in triple-negative breast cancer. Nat Genet 2022;54:459–68.
20. Kägi D, Ledermann B, Bürki K, Seiler P, Odermatt B, Olsen KJ, et al. Cytotoxicity mediated by T cells and natural killer cells is greatly impaired in perforin-deficient mice. Nature 1994;369:31–7.
21. Dalton DK, Pitts-Meek S, Keshav S, Figari IS, Bradley A, Stewart TA. Multiple defects of immune cell function in mice with disrupted interferon-gamma genes. Science 1993;259:1739–42.
22. Zijlstra M, Bix M, Simister NE, Loring JM, Raulet DH, Jaenisch R. Beta 2-microglobulin deficient mice lack CD4-8+ cytolytic T cells. Nature 1990;344:742–6.
23. Dull T, Zufferey R, Kelly M, Mandel RJ, Nguyen M, Trono D, et al. A third-generation lentivirus vector with a conditional packaging system. J Virol 1998;72:8463–71.
24. Dobin A, Davis CA, Schlesinger F, Drenkow J, Zaleski C, Jha S, et al. STAR: ultrafast universal RNA-seq aligner. Bioinformatics 2013;29:15–21.
25. Patro R, Duggal G, Love MI, Irizarry RA, Kingsford C. Salmon: fast and bias-aware quantification of transcript expression using dual-phase inference. Nat Methods 2017;14:417–9.
26. Zhu A, Ibrahim JG, Love MI. Heavy-tailed prior distributions for sequence count data: removing the noise and preserving large differences. Bioinformatics 2019;35:2084–92.
27. Ritchie ME, Phipson B, Wu D, Hu Y, Law CW, Shi W, et al. Limma powers differential expression analyses for RNA-sequencing and microarray studies. Nucleic Acids Res 2015;43:e47.
28. Federico A, Monti S. hypeR: an R package for geneset enrichment workflows. Bioinformatics 2020;36:1307–8.
29. Liberzon A, Birger C, Thorvaldsdóttir H, Ghandi M, Mesirov JP, Tamayo P. The Molecular Signatures Database (MSigDB) hallmark gene set collection. Cell Syst 2015;1:417–25.
30. Buenrostro JD, Wu B, Chang HY, Greenleaf WJ. ATAC-seq: a method for assaying chromatin accessibility genome-wide. Curr Protoc Mol Biol 2015;109:21.29.1–9.
31. Ewels PA, Peltzer A, Fillinger S, Patel H, Alneberg J, Wilm A, et al. The nf-core framework for community-curated bioinformatics pipelines. Nat Biotechnol 2020;38:276–8.
32. Heinz S, Benner C, Spann N, Bertolino E, Lin YC, Laslo P, et al. Simple combinations of lineage-determining transcription factors prime cis-regulatory elements required for macrophage and B cell identities. Mol Cell 2010;38:576–89.
33. Quinlan AR, Hall IM. BEDTools: a flexible suite of utilities for comparing genomic features. Bioinformatics 2010;26:841–2.
34. Liao Y, Smyth GK, Shi W. feature Counts: an efficient general purpose program for assigning sequence reads to genomic features. Bioinformatics 2014;30:923–30.
35. Thorvaldsdóttir H, Robinson JT, Mesirov JP. Integrative Genomics Viewer (IGV): high-performance genomics data visualization and exploration. Brief Bioinform 2013;14:178–92.
36. Ewels P, Magnusson M, Lundin S, Käller M. MultiQC: summarize analysis results for multiple tools and samples in a single report. Bioinformatics 2016;32:3047–8.
37. Berest I, Arnold C, Reyes-Palomares A, Palla G, Rasmussen KD, Giles H, et al. Quantification of differential transcription factor activity and multiomics-based classification into activators and repressors: diffTF. Cell Rep 2019;29:3147–59.e12.
38. Kulakovskiy IV, Vorontsov IE, Yevshin IS, Soboleva AV, Kasianov AS, Ashoor H, et al. HOCOMOCO: expansion and enhancement of the collection of transcription factor binding sites models. Nucleic Acids Res 2016;44:D116–25.
39. Wiśniewski JR, Zougman A, Nagaraj N, Mann M. Universal sample preparation method for proteome analysis. Nat Methods 2009;6:359–62.
40. Block J, Rashkova C, Castanon I, Zoghi S, Platon J, Ardy RC, et al. Systemic inflammation and normocytic anemia in DOCK11 deficiency. N Engl J Med 2023;389:527–39.

41. Metsalu T, Vilo J. ClustVis: a web tool for visualizing clustering of multivariate data using Principal Component Analysis and heatmap. Nucleic Acids Res 2015;43:W566–570.
42. Kärre K, Ljunggren HG, Piontek G, Kiessling R. Selective rejection of H–2-deficient lymphoma variants suggests alternative immune defence strategy. Nature 1986;319:675–8.
43. Naik SH, Perié L, Swart E, Gerlach C, van Rooij N, de Boer RJ, et al. Diverse and heritable lineage imprinting of early haematopoietic progenitors. Nature 2013;496:229–32.
44. Bai R, Chen N, Li L, Du N, Bai L, Lv Z, et al. Mechanisms of cancer resistance to immunotherapy. Front Oncol 2020;10:1290.
45. Sharma P, Hu-Lieskovan S, Wargo JA, Ribas A. Primary, adaptive, and acquired resistance to cancer immunotherapy. Cell 2017;168:707–23.
46. Zhou F. Molecular mechanisms of IFN-γ to up-regulate MHC class I antigen processing and presentation. Int Rev Immunol 2009;28:239–60.
47. Belkahla S, Brualla JM, Fayd'herbe de Maudave A, Falvo P, Allende-Vega N, Constantinides M, et al. The metabolism of cells regulates their sensitivity to NK cells depending on p53 status. Sci Rep 2022;12:3234.
48. Agresta L, Hoebe KHN, Janssen EM. The emerging role of CD244 signaling in immune cells of the tumor microenvironment. Front Immunol 2018;9:2809.
49. Ray A, Yuan C-Y, Miller NM, Mei H, Dittel BN. 2B4 is dispensable for T-dependent B cell immune responses, but its deficiency leads to enhanced T-independent responses due to an increase in peritoneal cavity B1b cells. PLoS One 2015;10:e0137314.
50. Brown DR, Calpe S, Keszei M, Wang N, McArdel S, Terhorst C, et al. Cutting edge: an NK cell-independent role for Slamf4 in controlling humoral autoimmunity. J Immunol 2011;187:21–5.
51. Shmerling M, Chalik M, Smorodinsky NI, Meeker A, Roy S, Sagi-Assif O, et al. LY6S, a new IFN-inducible human member of the Ly6a subfamily expressed by spleen cells and associated with inflammation and viral resistance. Immunohorizons 2022;6:253–72.
52. Luo L, McGarvey P, Madhavan S, Kumar R, Gusev Y, Upadhyay G. Distinct lymphocyte antigens 6 (Ly6) family members Ly6D, Ly6E, Ly6K and Ly6H drive tumorigenesis and clinical outcome. Oncotarget 2016;7:11165–93.
53. Mar KB, Rinkenberger NR, Boys IN, Eitson JL, McDougal MB, Richardson RB, et al. LY6E mediates an evolutionarily conserved enhancement of virus infection by targeting a late entry step. Nat Commun 2018;9:3603.
54. Acar A, Nichol D, Fernandez-Mateos J, Cresswell GD, Barozzi I, Hong SP, et al. Exploiting evolutionary steering to induce collateral drug sensitivity in cancer. Nat Commun 2020;11:1923.
55. Umkehrer C, Holstein F, Formenti L, Jude J, Froussios K, Neumann T, et al. Isolating live cell clones from barcoded populations using CRISPRa-inducible reporters. Nat Biotechnol 2021;39:174–8.
56. Baldwin LA, Bartonicek N, Yang J, Wu SZ, Deng N, Roden DL, et al. DNA barcoding reveals ongoing immunoediting of clonal cancer populations during metastatic progression and immunotherapy response. Nat Commun 2022;13:6539.
57. Goyal Y, Busch GT, Pillai M, Li J, Boe RH, Grody EI, et al. Diverse clonal fates emerge upon drug treatment of homogeneous cancer cells. Nature 2023;620:651–9.
58. Weinreb C, Rodriguez-Fraticelli A, Camargo FD, Klein AM. Lineage tracing on transcriptional landscapes links state to fate during differentiation. Science 2020;367:eaaw3381.
59. Chang MT, Shanahan F, Nguyen TTT, Staben ST, Gazzard L, Yamazoe S, et al. Identifying transcriptional programs underlying cancer drug response with TraCe-seq. Nat Biotechnol 2022;40:86–93.
60. Mittal D, Gubin MM, Schreiber RD, Smyth MJ. New insights into cancer immunoediting and its three component phases - elimination, equilibrium and escape. Curr Opin Immunol 2014;27:16–25.
61. Ljunggren HG, Kärre K. In serach of the "missing self": MHC molecules and NK cell recognition. Immunol Today 1990;11:237–44.
62. Weichold FF, Jiang Y, Dunn DE, Bloom M, Malkovska V, Hensel NF, et al. Regulation of a graft-versus-leukemia effect by major histocompatibility complex class II molecules on leukemia cells: HLA-DR1 expression renders K562 cell tumors resistant to adoptively transferred lymphocytes in severe combined immunodeficiency mice/nonobese diabetic mice. Blood 1997;90:4553–8.
63. Xing S, Ferrari de Andrade L. NKG2D and MICA/B shedding: a 'tag game' between NK cells and malignant cells. Clin Transl Immunology 2020;9:e1230.
64. Konjević GM, Vuletić AM, Mirjačić Martinović KM, Larsen AK, Jurišić VB. The role of cytokines in the regulation of NK cells in the tumor environment. Cytokine 2019;117:30–40.
65. Holmes C, Stanford WL. Concise review: stem cell antigen-1: expression, function, and enigma. Stem Cells 2007;25:1339–47.
66. Bradfute SB, Graubert TA, Goodell MA. Roles of Sca-1 in hematopoietic stem/progenitor cell function. Exp Hematol 2005;33:836–43.
67. Hordeaux J, Yuan Y, Clark PM, Wang Q, Martino RA, Sims JJ, et al. The GPI-linked protein LY6A drives AAV-PHP.B transport across the blood-brain barrier. Mol Ther 2019;27:912–21.
68. Park JW, Park JM, Park DM, Kim D-Y, Kim HK. Stem cells antigen-1 enriches for a cancer stem cell-like subpopulation in mouse gastric cancer. Stem Cells 2016;34:1177–87.
69. Li Y, Welm B, Podsypanina K, Huang S, Chamorro M, Zhang X, et al. Evidence that transgenes encoding components of the Wnt signaling pathway preferentially induce mammary cancers from progenitor cells. Proc Natl Acad Sci U S A 2003;100:15853–8.
70. Roarty K, Baxley SE, Crowley MR, Frost AR, Serra R. Loss of TGF-beta or Wnt5a results in an increase in Wnt/beta-catenin activity and redirects mammary tumour phenotype. Breast Cancer Res 2009;11:R19.
71. Batts TD, Machado HL, Zhang Y, Creighton CJ, Li Y, Rosen JM. Stem cell antigen-1 (Sca-1) regulates mammary tumor development and cell migration. PLoS One 2011;6:e27841.
72. Liu D, Xu C, Liu Y, Ouyang W, Lin S, Xu A, et al. A systematic survey of LU domain-containing proteins reveals a novel human gene, LY6A, which encodes the candidate ortholog of mouse Ly-6A/Sca-1 and is aberrantly expressed in pituitary tumors. Front Med 2023;17:458–75.
73. Al Hossiny M, Luo L, Frazier WR, Steiner N, Gusev Y, Kallakury B, et al. Ly6E/K signaling to TGF-β promotes breast cancer progression, immune escape and drug resistance. Cancer Res 2016;76:3376–86.
74. Zhao J, Jin D, Huang M, Ji J, Xu X, Wang F, et al. Glycolysis in the tumor microenvironment: a driver of cancer progression and a promising therapeutic target. Front Cell Dev Biol 2024;12:1416472.
75. Pflugh DL, Maher SE, Bothwell ALM. Ly-6 superfamily members Ly-6A/E, Ly-6C, and Ly-6I recognize two potential ligands expressed by B lymphocytes. J Immunol 2002;169:5130–6.
76. Shokouhifar A, Firouzi J, Nouri M, Sarab GA, Ebrahimi M. NK cell upraise in the dark world of cancer stem cells. Cancer Cell Int 2021;21:682.
77. Tsuchiya H, Shiota G. Immune evasion by cancer stem cells. Regen Ther 2021;17:20–33.